Received 30 June 2020; accepted 11 July 2020. Date of publication 22 July 2020; date of current version 21 August 2020.

Digital Object Identifier 10.1109/OJCOMS.2020.3010169

Performance Analysis of Energy Beamforming WPCN Links With Channel Estimation Errors

DANYANG WANG (Graduate Student Member, IEEE), AND CHINTHA TELLAMBURA (Fellow, IEEE)

Department of Electrical and Computer Engineering, University of Alberta, Edmonton, AB T6G 2R3, Canada

CORRESPONDING AUTHOR: C. TELLAMBURA (e-mail: ct4@ualberta.ca)

ABSTRACT In this paper, we analyze the performance of a wireless-powered communication network that consists of a multiple-antenna hybrid access point (AP) and a single-antenna user. The AP transmits radio frequency (RF) power in the downlink (DL) using maximal ratio transmission (MRT) type energy beamforming. The user harvests it and transmits data to the AP in the uplink (UL), which is received with maximal ratio combining (MRC). Previous analyses have assumed the availability of perfect channel estimation. In contrast, we eliminate this unrealistic assumption and consider the effect of imperfect channel estimates. We first derive the distributions of the received AP signal-to-noise ratio (SNR). We then analyze the average throughput performance of delay-limited and delay-tolerant modes by evaluating the outage probability (OP) and ergodic capacity (EC). We also derive the exact bit error rates (BERs) and symbol error rates (SERs) of several digital modulations. Asymptotic performance expressions in the high SNR regime and the large antenna regime are also developed. Finally, analytical and asymptotic results are validated by Monte-Carlo simulations. The impacts of the transmit power, the energy harvesting (EH) time, the number of antennas and the efficiency of EH are investigated.

INDEX TERMS Channel estimation errors, energy harvesting, average throughput, outage probability, ergodic capacity, symbol error rate.

I. INTRODUCTION

A. BACKGROUND AND MOTIVATION

WIRELESS energy harvesting communications may alleviate excess energy use of wireless networks [1]–[3]. They exploit the principles of microwave wireless energy transfer and may improve the energy efficiency of battery-constrained wireless nodes. Energy harvesting (EH) is feasible from various sources such as mechanical, solar, and radio-frequency (RF) energy sources. However, solar irradiance is susceptible to weather conditions and time varying. Mechanical motion is hard to predict [4]. In contrast, RF sources not only avoid those issues, but also are ubiquitous. For example, EH amounts of 5.5 μW and 2.3 μW are feasible at distances 15 m and 25 m from an RF source of 4 W and 1.78 W [5]. Applications of wireless-powered communication networks (WPCNs) include active radio-frequency identification (RFID), real-time location system tags, wireless sensors, and data loggers [6]. Moreover, Powercast has developed commercial WPCNs [7]. They could simplify the charging, servicing and maintenance of battery-needed devices [6], [8]–[10].

A key WPCN protocol is called harvest-then-transmit [11], which works in the following setup. follows. An access-point (AP) broadcasts RF power signals in the downlink (DL), users harvest energy and then transmit data to the AP in the uplink (UL). An alternative implementation is to deploy multiple power beacons (PBs), which are dedicated RF power transmitters for the purpose of enabling EH. These concepts have increased the interest in WPCNs, and thus [1] has discussed three different EH modes. The first is pure wireless power transfer (WPT), where an AP or a PB transmits power only to a wireless EH receiver, without any information exchange. The second mode is the WPCN, as described before. The third mode is simultaneous wireless information and power transfer (SWIPT). In SWIPT, a hybrid AP transmits energy and information using the same signal, from which the EH receiver will harvest energy and extract information. This paper focuses on

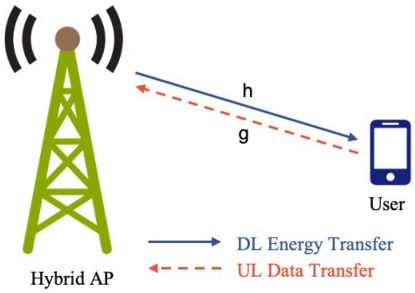

FIGURE 1. System Model.

the second mode, namely the WPCN, a prototype of which is shown in Fig. 1. This prototype consists of a multiple-antenna hybrid AP and a single-antenna user. The AP can utilize its multiple antennas to focus energy in the direction of the user; energy beamforming is thus common place to increase both wireless power transfer efficiency and data transfer efficiency [1], [9], [10].

B. PERFORMANCE WITH PERFECT CSI

Before proceeding to the main issue of imperfect CSI, we briefly review a few works on WPCNs with perfect CSI [9], [10], [12]–[14]. The key paper, which is the starting point of our work, is [9]. This work analyzes the average throughput of the same WPCN (Fig. 1) for two transmission modes. It utilizes maximum ratio transmission (MRT) energy beamforming to extend coverage and to maximize the amount of harvested energy. This work also develops asymptotic analyses in the high signal-to-noise ratio (SNR) regime. While [12] derives the outage probability, ergodic capacity, achievable throughput and bit error rate (BER) using Meijer G-function for the generalized $\kappa-\mu$ fading channel. However, this study is limited to single-antenna AP and user. The focus of this paper is to derive unified expressions, which can handle the three classical fading models - namely Rayleigh, Rician and Nakagami-m. The interplay between EH and user cooperation in a WPCN is the focus of [10], which optimizes the energy beamforming vector and time and power allocations. The time correlation between the DL and UL channels is investigated in terms of the BER and achievable rate [13]. In [15], the energy efficiency is maximized by jointly optimizing energy transfer time duration and transmit power. The average throughput of a multiple-input multiple-output (MIMO) WPCN has been studied in [14]. All these works assume the availability of perfect CSI, which is the critical difference from our paper.

C. PERFORMANCE WITH IMPERFECT CSI

CSI is an absolutely critical component of wireless links. On the other hand, in practical systems, perfect CSI is not available and in fact imperfect CSI is the norm [16]–[19]. Typically, training (pilot) symbols are sent periodically for CSI estimation purposes [20]. Alternatively, blind and semi-blind techniques have also been developed. The impact of CSI estimation errors includes the loss of diversity and capacity gains. To understand this, we can consider a simple wireless link with one transmit antenna and say $N > 1$ receive antennas with maximal ratio combining (MRC) reception. The antenna separation is sufficient to ensure independent fading across them. Now if CSI is perfect, the diversity order of this link is N. In contrast, for imperfect CSI, the diversity order collapses to one [21], [22].

Although imperfect CSI for WPCNs is studied in several studies [23]–[32], these works focus on specific application scenarios and associated optimizations. For example, in [23] the EH process is optimized by considering beamforming design, power allocation, antenna selection and time division based on imperfect CSI. On the other hand, how secrecy performance and resource allocation issues are affected by imperfect CSI has also been investigated [24], [25]. The focus of [26] is the capacity of an EH link Rician fading channels for two cases: absence of CSI and partial CSI. Throughput optimization of a massive MIMO WPCN with estimated CSI has also been investigated [27]. The impact of CSI on wireless powered relaying (WPR) systems, a form of WPCNs, has also been studied [28], [29]. The paper [28] investigates the impact of CSI and antenna correlation considering instantaneous or statistical CSI and derives outage probability and ergodic capacity. The focus of [29] is the effect of the non-linear EH process and imperfect CSI. Reference [30] analyzes an EH cooperative communication link for two cases: (a) a single-antenna source with perfect CSI and (b) a multiple-antenna source with imperfect CSI. The uplink scheduling problem for an AP with imperfect CSI has been investigated [31]. The result is a discrete optimization solution of the best transmission schedule. Secrecy throughput optimization of a WPCN with nonlinear EH has been studied in [32]. It considers both perfect and imperfect CSI cases.

Although the aforementioned works consider imperfect CSI, their primary perspective is not that of a comprehensive performance analysis (e.g., deriving outage, capacity and error rates). Instead, they focus on several application domains and optimization. Thus, an analysis of imperfect CSI on the performance of WPCNs has been missing. Thus, this topic is the focus of the present paper.

D. HIGH-SNR ANALYSIS

Another missing factor is the high SNR analysis of WPCNs with imperfect CSI. To explain the reason for this, we need some background. For a standard point-to-point communication link subject to small-scale fading, the SNR at the receiver may be represented as $\gamma = X\overline{\gamma}$, where $\overline{\gamma}$ is the unfaded SNR, a constant, and X is a random variable that accounts for all the effects of small-scale fading [33]. It thus has the PDF (probability density function), say, $f(x)$. Suppose the Taylor series near $x = 0$ to be $f(x) = a_0x^t + a_1x^{t+1} + \ldots$. It turns out that the asymptotic performance depends on just the first term of the Taylor series and the two parameters $a_0 > 0$ and $t \geq 0$ are critical. First developed in [33], the

insight is that as $\overline{\gamma} \to \infty$, the asymptotic performance can be expressed as

$$P_e(\overline{\gamma}) = (G_c \overline{\gamma})^{-G_d}, \tag{1}$$

where G_c and G_d, which are functions of a and t, are called coding gain and diversity gain, respectively. These important, widely-used parameters enable the design and optimization of wireless systems. For instance, from (1), we observe that $\log[P_e(\overline{\gamma})]$ varies linearly with $\log[\overline{\gamma}]$, which provides direct insights in terms of coding gain and diversity gain. From (1), we can readily see that

$$G_d = \lim_{\bar{\gamma} \to \infty} \frac{-\log P_e(\bar{\gamma})}{\log \bar{\gamma}}.$$

This limiting process can be used with any outage or error rate expression to determine the diversity order.

Since the seminal paper [33], several improvements have been found [34]–[36]. Instead of the single term expansion, [34] considers $f(\beta) = a_0 x^t + a_1 x^{t+1}$, which are the first two terms of the Taylor series, and approximate this as an exponential function. This approach leads to a very highly accurate asymptotic performance expressions, albeit more complicated than those derived based on [33]. A Mellin transform based approach over the asymptotic expansion of the PDF, given in (1) to derive a uniform approximation [35] that works for both low and high SNR regimes. Authors in [36] combined dual exponential sum with the asymptotic model in (1).

E. PROBLEM STATEMENT AND CONTRIBUTIONS

To the best of our knowledge, the performance degradation of the WPCN (Fig. 1) due to imperfect CSI has thus far not been characterized. This gap in understanding is problematic because, as mentioned before, imperfect CSI can lead to performance losses. To characterize the impact of this problem, we investigate the throughput performances and bit/symbol error rates of several modulations, as well as their high SNR performance of this WPCN with energy beamforming and imperfect CSI. The throughput performance is analyzed for both delay-limited and delay-tolerant modes. These modes correspond to the length of the codewords transmitted by the user. In the delay-limited mode, multiple codewords fit the duration of each transmission block, and thus the AP decodes each codeword as it arrives. In this case, outage probability (OP), the probability that the short-term information transfer rate falls below the fixed transmission rate of the user, serves as a critical measure of the average throughput.

On the other hand, in the delay-tolerant mode, the user can tolerate more delay and thus can use long codewords compared to the duration of the transmission block. In this case, it is best for the AP to store multiple signal blocks in a buffer and to decode them together. Consequently, the ergodic capacity (EC), which is the long-term average of the instantaneous information transfer rate, is the relevant measure of the system throughput.

The main contributions are summarized as follows:

1) In practical networks, perfect CSI is not available due to estimation errors, feedback delays and other issues [23]. Thus, it is important to include these effects in the analysis of performance. To this end, for a WPCN with imperfect CSI, we derive the PDF and CDF (cumulative distribution function) and moment generating function (MGF) of the received SNR at the AP and the exact close-form throughput expressions for both delay-limited and delay-tolerant modes.
2) BER and SER values quantify the reliability of the network. Thus, we also derive exact close-form expressions for binary phase shift keying (BPSK), binary differential phase shift keying (BDPSK), M-ary phase shift keying (M-PSK), and M-ary quadrature amplitude modulation (M-QAM).
3) As will be seen later, the PDF of the received SNR $f(x)$ contains Bessel functions, which lack a simple Taylor series expansion at $x = 0$. For this reason, the classical asymptotic approach [33] appears intractable here. Thus, we develop a two-step process, exploiting the fact that the received SNR is the product of two random variables (RVs). So we take the expectation over one RV first and simplify the result to yield asymptotic results. By using this general idea, we derive novel, asymptotic (i.e., high-SNR) expressions of throughput, BERs, and SERs. For the delay-tolerant mode, the asymptotic large antenna case and the throughput-optimal EH time in the high SNR regime are also derived.
4) Finally, numerical results and simulations are presented to validate the derived results and to investigate the interplay between the quality of CSI and the EH process. We thus find the large number of antennas eliminates the effects of small-scale fading. We also find that the quality of CSI measured by ρ has more impact on the system performance than the other factors.

In a nutshell, this paper generalizes the work of [9] to the imperfect CSI case. As well, [9] does not consider the analysis of BER/SER, which is a main part of this paper.

Notation: For random variable X, $f_X(\cdot)$ and $F_X(\cdot)$ denote PDF and CDF. Vector $\mathbf{x} \sim \mathcal{CN}(\boldsymbol{\mu}, \boldsymbol{\Sigma})$ denotes a circularly symmetric complex Gaussian vector with mean $\boldsymbol{\mu}$ and covariance matrix $\boldsymbol{\Sigma}$. The special case is the circularly symmetric complex Gaussian RV with mean μ and variance σ^2 denoted by $x \sim \mathcal{CN}(\mu, \sigma^2)$. The gamma function $\Gamma(a)$ is given in [37, eq. (8.310.1)]; $K_\nu(\cdot)$ is the ν-th order modified Bessel function of the second kind [37, eq. (8.432)]; $G_{pq}^{mn}(z \mid \begin{smallmatrix} a_1 \cdots a_p \\ b_1 \cdots b_q \end{smallmatrix})$ denotes the Meijer G-function [37, eq. (9.301)]; $\psi(\cdot)$ is the Euler psi function [37, eq. (8.36)]; x^H denotes the transpose and conjugate of x; $W_{\lambda,\mu}(\cdot)$ is the Whittaker function, [37, eq. (9.200)]; $\Psi(a, b; z)$ is the confluent hypergeometric function in [37, eq. (9.211.4)].

This paper is organized as follows. In Section II, we describe the system model and the received SNR at the AP.

Section III presents several statistical distribution results, which are necessary for the performance analysis of the WPCN. Section IV obtains the exact performance and asymptotic results for average throughput of delay-limited and delay-tolerant modes. In Section V, average BERs of BPSK and BDPSK and average SERs of coherent M-PSK and coherent square M-QAM are analyzed as closed-form and asymptotic results. In Section VI, numerical results show the accuracy of the exact and asymptotic results. Section VII concludes the paper. Finally, some derivations are relegated to Appendix.

II. SYSTEM MODEL

We first describe the network model in Fig. 1, which consists of a single-antenna user and a multiple-antenna hybrid AP. These two are half-duplex nodes. The AP has $N \geq 1$ antennas and uses MRC for signal reception. The user, without a battery, is powered via the harvest-then-transmit protocol [9]. Thus, the energy transfer channel, i.e., the AP-to-user channel, is denoted as $\mathbf{h} = [h_1, \ldots, h_k, \ldots, h_N]^T \in \mathbb{C}^{N\times 1}$, and the data transfer channel, i.e., user-to-AP channel, is denoted as $\mathbf{g} = [g_1, \ldots . g_k, \ldots, g_N]^T \in \mathbb{C}^{N\times 1}$. The channel coefficients $h_k, g_k \, \forall k \in [1, N]$ are independent and identically distributed (i.i.d.) circularly symmetric complex Gaussian random variables with zero-mean and unit-variance, i.e., $h_k, g_k \sim \mathcal{CN}(0, 1)$. Equivalently, the channel coefficient magnitudes $|h_k|$ and $|g_k|$ $(k = 1, \ldots, N)$ are distributed with the Rayleigh PDF, i.e., $f(x) = 2xe^{-x^2}$, $0 \leq x < \infty$.

Let channel estimates of the true channels $\mathbf{h}$ and $\mathbf{g}$ be denoted as $\hat{\mathbf{h}}$ and $\hat{\mathbf{g}}$, respectively. AP gets them via suitable pilot-assisted channel estimation techniques. Thus, these estimate will have both noise and correlative components. These are represented in the following model. For any true channel $\mathbf{x} \in \{\mathbf{h}, \mathbf{g}\}$, the channel estimate $\hat{\mathbf{x}} \in \{\hat{\mathbf{h}}, \hat{\mathbf{g}}\}$ is related as [18]

$$\hat{\mathbf{x}} = \rho\mathbf{x} + \sqrt{1-\rho^2}\tilde{\mathbf{n}}, \tag{2}$$

where $0 \leq \rho \leq 1$ is the correlation coefficient between a true channel and its estimate, and $\tilde{\mathbf{n}} \in \mathbb{C}^{N\times 1}$ is an N-dimensional noise vector of i.i.d. $\mathcal{CN}(0, 1)$ entries. The quality of CSI is indicated by the value of ρ. While $\rho = 1$ and $\rho = 0$ cases indicate perfect and worst-case (noisy) channel estimation scenarios. The range $0 \leq \rho < 1$ will be the imperfect CSI case. The exact value of ρ in practice is a function of pilot symbols and their power. For convenience, we assume both UL and DL estimations are characterized by the same value of ρ. It is worth mentioning that the model (2) also represents the case of outdated CSI as well. In this case, the well-known Jake's model suggests that $\rho = J_0(2\pi f_d \tau)$, where $J_0(x)$ denotes the zeroth order Bessel function of first kind and f_d indicates the maximum Doppler frequency and τ is the time delay. Thus, all these factors can be investigated in conjunction with the EH process, a task that is left for future research.

Given these details of channel estimation, we next turn to specify the amount of harvested energy at the AP. Without loss of generality, we assume a unit transmission block $(T = 1)$. Thus, for τ duration, where $\tau \in (0, 1)$, the AP transmits RF power at level P in the DL and the user harvests it. The user then transmits data in the UL for $(1-\tau)$ duration. This cycle repeats again in the next block and so on. We assume that the AP processes the transmit power symbols with a linear precoder to achieve energy beamforming. Energy beamforming is the process of a highly directional transmission with high-gain antennas to focus energy beams toward the user. It thus maximizes the harvested energy at the user. To achieve this, the transmit signals at different antennas are carefully weighted (precoding) to achieve constructive superposition at the user. The precoding vector is computed by the AP, which requires accurate CSI. In this work, we assume MRT energy beamforming, which is optimal for the single-cell case [1]. Thus, the AP transmit signal is $\sqrt{P}\mathbf{f}$ where the precoding vector $\mathbf{f}$ is chosen subject to the constraint $||\mathbf{f}|| = 1$. The AP will utilize imperfect CSI to compute $\mathbf{f} = \frac{\hat{\mathbf{h}}}{|\hat{\mathbf{h}}|}$. Thus, the user's total harvested energy is $E_h = \eta\tau|\sqrt{P}\mathbf{f}^H\mathbf{h}|^2 = \eta\tau P\frac{||\hat{\mathbf{h}}^H\mathbf{h}||^2}{\hat{\mathbf{h}}^H\hat{\mathbf{h}}}$ [23, eq. (2)], where η is the energy conversion efficiency. In practice, the maximum conversion efficiency depends on the specific technologies; for example, it is about 48% with a Schottky diode and around 56% with CMOS (complementary metal-oxide-semiconductor) devices [38].

By using the harvested energy, the user transmits data signals to the AP in the UL with power P_s that is given as

$$P_s = \frac{E_h}{1-\tau} = \frac{\tau\eta P}{1-\tau}\frac{\left|\hat{\mathbf{h}}^H\mathbf{h}\right|^2}{\hat{\mathbf{h}}^H\hat{\mathbf{h}}}. \tag{3}$$

Note that if perfect CSI is available, then $\hat{\mathbf{h}} = \mathbf{h}$. The transmit power of the user then becomes $P_s = \frac{\tau\eta P}{1-\tau}||\mathbf{h}||^2$, which is consistent with previous results [9]. The received signal at the AP is $y_A = \sqrt{P_s}\mathbf{g}s + \mathbf{n}$, where s is the energy-normalized data symbol and $\mathbf{n}$ is the complex additive white Gaussian noise (AWGN) term, $\mathbf{n} \sim \mathcal{CN}(0, 1)$. The AP uses MRC type reception to maximize the received SNR; with MRC, the received signal is multiplied by $\hat{\mathbf{g}}^H$. This multiplication will affect both the signal term and noise term in y_A. But the ratio of the powers of these two terms gets scaled by $\frac{||\hat{\mathbf{g}}^H\mathbf{g}||^2}{\hat{\mathbf{g}}^H\hat{\mathbf{g}}}$. The SNR at the AP can thus be derived as

$$\gamma_A = \frac{\tau\eta P}{1-\tau}\frac{1}{\sigma^2}\frac{\left|\hat{\mathbf{h}}^H\mathbf{h}\right|^2}{\hat{\mathbf{h}}^H\hat{\mathbf{h}}}\frac{||\hat{\mathbf{g}}^H\mathbf{g}||^2}{\hat{\mathbf{g}}^H\hat{\mathbf{g}}} = c\overline{\gamma}XY, \tag{4}$$

where σ^2 is the power of noise, $\overline{\gamma} = \frac{P}{\sigma^2}$, $c = \frac{\tau\eta}{1-\tau}$, $X = \frac{||\hat{\mathbf{h}}^H\mathbf{h}||^2}{\hat{\mathbf{h}}^H\hat{\mathbf{h}}}$, and $Y = \frac{||\hat{\mathbf{g}}^H\mathbf{g}||^2}{\hat{\mathbf{g}}^H\hat{\mathbf{g}}}$. It is clear that both X and Y have the identical statistical distribution. These ratios arise in the performance evaluation of MRC diversity reception with imperfect CSI, and their distribution was derived in a classical paper [21].

III. STATISTICAL DISTRIBUTION RESULTS

This section provides necessary statistical distributions for the use in subsequent derivations throughout the paper.

A. THE DISTRIBUTION OF RECEIVED SNR, γ_A

Lemma 1: Since $\gamma_A = c\overline{\gamma}XY$, the PDF of γ_A is the product of a constant and the RV $Z = XY$. Therefore, the PDF can be given by

$$f_{\gamma_A}(z) = \sum_{n=1}^{N}\sum_{m=1}^{N} \frac{2B(m,n)\left(\frac{z}{c\overline{\gamma}}\right)^{\alpha(m,n)}}{c\overline{\gamma}} K_{n-m}\left(2\sqrt{\frac{z}{c\overline{\gamma}}}\right), \quad (5)$$

where N is the number of antennas at the AP, $\alpha(m,n) = \frac{n+m-2}{2}$, $A(n) = \binom{N-1}{n-1}\frac{(1-\rho^2)^{N-n}}{\Gamma(n)}\rho^{2(n-1)}$ and $B(m,n) \triangleq A(n)A(m)$.

Proof: The PDF of X was derived in [21]

$$f_X(x) = \sum_{n=1}^{N} A(n)x^{n-1}e^{-x}, \quad 0 \le x < \infty. \quad (6)$$

As channels are i.i.d., the PDF of Y, $f_Y(y)$, can also be given as (6).

Then the PDF of the product of two non-negative RVs X and Y, denoted as $Z = XY$, can be derived as

$$\begin{aligned} f_Z(z) &\overset{(a)}{=} \int_0^\infty \frac{1}{\omega} f_X(\omega) f_Y\left(\frac{z}{\omega}\right) d\omega \\ &\overset{(b)}{=} \sum_{n=1}^{N}\sum_{m=1}^{N} \frac{B(m,n)}{z^{-(m-1)}} \int_0^\infty \omega^{n-m-1} e^{-\omega-\frac{z}{\omega}} d\omega \\ &\overset{(c)}{=} \sum_{n=1}^{N}\sum_{m=1}^{N} 2B(m,n) z^{\frac{n+m-2}{2}} K_{n-m}\left(2\sqrt{z}\right), \end{aligned} \quad (7)$$

where (a) is the formula to find the PDF of the product of two RVs; (b) is obtained by (6); (c) is due to [37, eq. (3.471.9)].

Since $\gamma_A = c\overline{\gamma}Z$, the PDF of γ_A can be derived as (5). ■

Corollary 1: The CDF of γ_A is given by

$$\begin{aligned} F_{\gamma_A}(x) = &\sum_{n=1}^{N}\sum_{m=1}^{N} \frac{B(m,n)}{(c\overline{\gamma})^{(\alpha(m,n)+1)}} x^{\alpha(m,n)+1} \\ &\times G_{1,3}^{2,1}\left(\frac{x}{c\overline{\gamma}}\middle| \begin{matrix} -\alpha(m,n) \\ \frac{n-m}{2}, -\frac{n-m}{2}, -\alpha(m,n)-1 \end{matrix}\right). \end{aligned} \quad (8)$$

Proof:

$$\begin{aligned} F_{\gamma_A}(x) &\overset{(a)}{=} \sum_{n=1}^{N}\sum_{m=1}^{N} \frac{2B(m,n)}{c\overline{\gamma}} \\ &\quad \times \int_0^x \left(\frac{z}{c\overline{\gamma}}\right)^{\alpha(m,n)} K_{n-m}\left(2\sqrt{\frac{z}{c\overline{\gamma}}}\right) dz \\ &\overset{(b)}{=} \sum_{n=1}^{N}\sum_{m=1}^{N} \frac{B(m,n)}{(c\overline{\gamma})^{(\alpha(m,n)+1)}} x^{\alpha(m,n)+1} \\ &\quad \times G_{1,3}^{2,1}\left(\frac{x}{c\overline{\gamma}}\middle| \begin{matrix} -\alpha(m,n) \\ \frac{n-m}{2}, \frac{m-n}{2}, -\alpha(m,n)-1 \end{matrix}\right), \end{aligned} \quad (9)$$

where (a) follows from the definition of CDF; (b) is obtained by using the equation which expresses $K_\nu(\cdot)$ in terms of $G_{p,q}^{m,n}[\cdot]$ in [9] and [37, eq. (9.31.5)]. ■

In addition to the PDF and CDF, the MGF can also be used to evaluate performance measures [39] and their high-SNR approximations [33]. For these reasons, we next derive the MGF of γ_A in detail.

B. MOMENTS-GENERATING FUNCTION

Lemma 2: The MGF of γ_A can be given by

$$\begin{aligned} M_{\gamma_A}(t) = &\sum_{n=1}^{N}\sum_{m=1}^{N} B(m,n)\left(\frac{1}{c\overline{\gamma}}\right)^{\alpha(m,n)+\frac{1}{2}} \\ &\times \Gamma(n)\Gamma(m) e^{\frac{1}{2tc\overline{\gamma}}} t^{-\frac{1}{2}-\alpha(m,n)} W_{-\frac{1}{2}-\alpha(m,n),\frac{n-m}{2}}\left(\frac{1}{tc\overline{\gamma}}\right). \end{aligned} \quad (10)$$

Proof: The MGF is defined as $M_{\gamma_A}(t) = \mathbb{E}[e^{-t\gamma_A}]$. By substituting (5) in this definition, we find

$$\begin{aligned} M_{\gamma_A}(t) &= \int_0^\infty e^{-ty} f_{\gamma_A}(y) dy \\ &\overset{(a)}{=} \sum_{n=1}^{N}\sum_{m=1}^{N} \frac{2B(m,n)}{c\overline{\gamma}}\left(\frac{1}{c\overline{\gamma}}\right)^{\alpha(m,n)} \\ &\quad \times \int_0^\infty e^{-ty} y^{\alpha(m,n)} K_{n-m}\left(2\sqrt{\frac{1}{c\overline{\gamma}}y}\right) dy, \end{aligned} \quad (11)$$

where (a) follows by using the PDF of γ_A; (10) is then obtained by applying [37, eq. (6.643.3)]. ■

Corollary 2: Since the MGF in Lemma 2 is a complicated expression, the effect of different parameters on the MGF is hard to see directly. To alleviate this issue, we derive the asymptotic (e.g., $\overline{\gamma} \to \infty$) MGF as

$$\begin{aligned} M_{\gamma_A}^{asy}(t) \approx &\sum_{m=1}^{N} \frac{B(m,1)}{tc\overline{\gamma}} \\ &\times \left[\sum_{k=1}^{m-1} \Gamma(k)\left(-\frac{1}{tc\overline{\gamma}}\right)^{m-1-k} \right. \\ &\left. + (-1)^{m-2} e^{\frac{1}{tc\overline{\gamma}}}\left(\frac{1}{tc\overline{\gamma}}\right)^{m-1} E_i\left(-\frac{1}{tc\overline{\gamma}}\right)\right], \end{aligned} \quad (12)$$

where $E_i(\cdot)$ is the exponential integral function [37, eq. (8.211.1)].

Proof: Let us revisit the definition of the MGF; $M_{\gamma_A}(t) = \mathbb{E}[e^{-t\gamma_A}]$. Since γ_A is a product of X and Y, we first take the expectation of MGF over X. Thus, the MGF conditional on Y, denoted as $M_{\gamma_A|Y}(t)$, is given by

$$\begin{aligned} M_{\gamma_A|Y}(t) &= \mathbb{E}\left[e^{-tc\overline{\gamma}XY}\right] \\ &= \sum_{n=1}^{N} \frac{A(n)\Gamma(n)}{(1+tc\overline{\gamma}Y)^n}. \end{aligned} \quad (13)$$

This expression (13) is derived by taking the expectation over the PDF of X, which is given by (6).

The next step is to take the expectation over Y, which yields

$$M_{\gamma_A}(t) = \sum_{n=1}^{N}\sum_{m=1}^{N} B(m,n)\Gamma(n)\int_0^\infty \frac{y^{m-1}e^{-y}}{(1+tc\overline{\gamma}y)^n}dy. \quad (14)$$

We next note that (14) has the series sum over n and m. If we expand the series over different n values, when $\overline{\gamma}\to\infty$, the integrals for which $n\geq 2$ can be negligible compared to the one for $n=1$. For this reason, (14) can be fairly accurately approximated as follows:

$$\begin{aligned} M_{\gamma_A}^{asy}(t) &\approx \sum_{m=1}^{N} B(m,1)\int_0^\infty \frac{y^{m-1}e^{-y}}{1+tc\overline{\gamma}y}dy, \\ &\overset{(a)}{=} \sum_{m=1}^{N}\frac{B(m,1)}{tc\overline{\gamma}} \\ &\quad\times\left[\sum_{k=1}^{m-1}\Gamma(k)\left(-\frac{1}{tc\overline{\gamma}}\right)^{m-1-k}\right. \\ &\quad\left.+(-1)^{m-2}e^{\frac{1}{tc\overline{\gamma}}}\left(\frac{1}{tc\overline{\gamma}}\right)^{m-1}E_i\left(-\frac{1}{tc\overline{\gamma}}\right)\right], \end{aligned} \quad (15)$$

where (a) is derived by using [37, eq. (3.353.5)]. ∎

While the asymptotic MGF of γ_A given in (15) is fairly simplified compared to the exact one (10), even simper version is possible. There are two cases: imperfect CSI and perfect CSI. These are given in the next corollary.

Corollary 3: The asymptotic result in (15) can be further simplified for the case of imperfect CSI as

$$M_{\gamma_A}^{asy}(t) \approx \left(1-\rho^2\right)^{2(N-1)}\frac{\left[\ln(ct\overline{\gamma})-\gamma_{EM}\right]}{ct\overline{\gamma}}, 0\leq\rho<1, \quad (16)$$

where γ_{EM} is the Euler-Mascheroni constant. If perfect CSI is available, then the MGF is approximately

$$M_{\gamma_A}^{asy}(t) \approx (tc\overline{\gamma})^{-N}\Psi\left(N,1;\frac{1}{tc\overline{\gamma}}\right), \quad \rho=1, \quad (17)$$

where $\Psi(a,b;z)$ is known as Tricomi's confluent hypergeometric function or the confluent hypergeometric function of the second kind [37, eq. (9.211.4)].

Proof: For the imperfect CSI case, when $0\leq\rho<1$, in (14), the dominant part is the one with $n=1$ and $m=1$. Therefore, we can consider just that term of (14) as

$$\begin{aligned} M_{\gamma_A}^{asy}(t) &= \left(1-\rho^2\right)^{2(N-1)}\int_0^\infty\frac{e^{-y}}{1+xy}dy \\ &\overset{(a)}{=} \left(1-\rho^2\right)^{2(N-1)}\frac{e^{\frac{1}{x}}\Gamma\left(0,\frac{1}{x}\right)}{x}, \end{aligned} \quad (18)$$

where $x=ct\overline{\gamma}$ and $\Gamma(s,x)$ is upper incomplete gamma function [37, eq. (8.350.2)]. Let $U=\frac{1}{x}e^{\frac{1}{x}}\Gamma(0,\frac{1}{x})$. By using the series expansion of U at $x=\infty$, we can show that

$$U=\frac{-\gamma_{EM}+\ln(x)}{x}+O\left(\frac{1}{x^2}\right).$$

When $\overline{\gamma}\to\infty$, we have $\frac{1}{x}\to 0$. Therefore, U is approximated well by the first term on the right. We thus find

$$M_{\gamma_A}^{asy}(t) = \frac{\left(1-\rho^2\right)^{2(N-1)}\left[\ln(ct\overline{\gamma})-\gamma_{EM}\right]}{(ct\overline{\gamma})}+O\left(\frac{1}{\overline{\gamma}^2}\right). \quad (19)$$

For the case of perfect CSI , where $\rho=1$, the coefficient $A(n)$ is zero for all n, except for $n=N$. Therefore $B(m,n)$ exists only when $m=n=N$. So when $\rho=1$, the MGF may be expressed as

$$\begin{aligned} M_{\gamma_A}^{asy}(t) &= \frac{1}{\Gamma(N)}\int_0^\infty\frac{y^{N-1}e^{-y}}{(1+tc\overline{\gamma}y)^N}dy \\ &\overset{(a)}{=} (tc\overline{\gamma})^{-N}\Psi\left(N,1;\frac{1}{tc\overline{\gamma}}\right), \end{aligned} \quad (20)$$

where (a) is obtained by [37, eq. (9.211.4)]. ∎

Thus far, we have covered the basic distributional results. Next, we will derive the SNR for the large antenna regime ($N\to\infty$).

C. SNR FOR THE LARGE ANTENNA CASE

The following corollary finds the deterministic limit of the SNR as the number of antennas becomes extremely large. This result is essential for the throughput analysis of the delay-tolerant mode.

Corollary 4: In this case, we consider the number of AP antenna increases without limitation with a fixed $\overline{\gamma}$. Then γ_A can be derived as

$$\gamma_A \approx \frac{\tau\eta}{1-\tau}\overline{\gamma}\rho^4N^2. \quad (21)$$

It is observed from (21), the effect of small-scale fading has vanished when the number of AP antenna is very large. This effect is known as channel hardening due to the impact of large scale spatial diversity [40]. Note that γ_A also increases with the increment of energy conversion efficiency η, $\overline{\gamma}$, correlation coefficient ρ and the number AP of antennas.

Proof: The channel coefficients are i.i.d. circularly symmetric complex Gaussian RVs with zero-mean and unit-variance, so $\hat{\mathbf{h}}\sim\mathcal{CN}(0,I)$.

$$\begin{aligned} \frac{\hat{\mathbf{h}}^H\mathbf{h}}{N} &\overset{(a)}{=} \frac{1}{N}\left(\rho\mathbf{h}+\sqrt{1-\rho^2}\tilde{\mathbf{n}}\right)^H\mathbf{h} \\ &\overset{(b)}{=} \frac{\rho\mathbf{h}^H\mathbf{h}}{N}+\frac{\sqrt{1-\rho^2}\tilde{\mathbf{n}}^H\mathbf{h}}{N} \\ &\overset{(c)}{\approx} \rho, \end{aligned} \quad (22)$$

where in step (a), we substitute the definition of $\hat{\mathbf{h}}$ (2) in $\hat{\mathbf{h}}^H\mathbf{h}$. Step (c) follows from the law of large numbers, $\frac{\mathbf{h}^H\mathbf{h}}{N}\xrightarrow{a.s.}1$, as $N\to\infty$ [41, eqs. (7.14) and (7.15)]. Similarly, $\frac{\hat{\mathbf{g}}^H\mathbf{g}}{N}\xrightarrow{a.s.}\rho$, where $\xrightarrow{a.s.}$ denotes the almost sure convergence.

So we can obtain $X=\frac{||\hat{\mathbf{h}}^H\mathbf{h}||^2}{\hat{\mathbf{h}}^H\hat{\mathbf{h}}}\xrightarrow{a.s.}\rho^2N$ and $Y=\frac{||\hat{\mathbf{g}}^H\mathbf{g}||^2}{\hat{\mathbf{g}}^H\hat{\mathbf{g}}}\xrightarrow{a.s.}\rho^2N$. Therefore, $\gamma_A\xrightarrow{a.s.}\frac{\tau\eta}{1-\tau}\overline{\gamma}\rho^4N^2$. ∎

IV. AVERAGE THROUGHPUT ANALYSIS

In this section, we evaluate the average throughput performance of the system model (Section II) We consider both delay-limited mode and delay-tolerant mode. The performance metrics OP and EC are analyzed for these modes. Moreover, we analyze the asymptotic performance at high SNR regime to gain more insights.

A. DELAY-LIMITED TRANSMISSION MODE

1) EXACT THROUGHPUT ANALYSIS

In this section, we consider the delay-limited case, where the AP decodes the received signals one codeword at a time. Therefore, the throughput is now measured by the OP, which is the probability that the instantaneous channel capacity falls below the fixed rate R bits/s/Hz, where R is the fixed transmission rate of the user. The OP is thus given by

$$P_{out} = \Pr\big(\log_2(1+\gamma_A) < R\big) = F_{\gamma_A}(\gamma_{th}), \tag{23}$$

where $\gamma_{th} = 2^R - 1$ and $F_{\gamma_A}(y)$ is the CDF of γ_A given in (8). The user transmits for an effective communication time fraction $(1-\tau)$ during the each harvest and transmit cycle. Therefore, the average throughput of the delay-limited transmission mode in bits/s/Hz is

$$\begin{aligned} R_{DL} &= (1-P_{out})(1-\tau)R \\ &= R^*\Bigg[1 - \sum_{n=1}^{N}\sum_{m=1}^{N} \frac{B(m,n)}{(c\overline{\gamma})^{(\alpha(m,n)+1)}} {\gamma_{th}}^{\alpha(m,n)+1} \\ &\quad \times G_{1,3}^{2,1}\left(\frac{\gamma_{th}}{c\overline{\gamma}}\middle| \begin{matrix} -\alpha(m,n) \\ \frac{n-m}{2}, \frac{m-n}{2}, -\alpha(m,n)-1 \end{matrix}\right)\Bigg], \end{aligned} \tag{24}$$

where $R^* = (1-\tau)R$.

Although the throughput expression (24) is closed form, it consists of the Meijer G-function, which does not directly reveal specific relationships between the throughput and the parameters ρ, τ, and $\overline{\gamma}$. That motivates the asymptotic analysis.

2) ASYMPTOTIC THROUGHPUT ANALYSIS

In order to gain a simpler result, we derive the asymptotic throughput.

Proposition 1: When $\overline{\gamma} \to \infty$, the asymptotic throughput in bits/s/Hz is given by

$$R_{DL} = R^*\Bigg[1 - 2\sum_{n=1}^{N}\sum_{m=1}^{N} B(m,n)\Delta^{\frac{m+n}{2}} K_{n-m}\Big(2\sqrt{\Delta}\Big)\Bigg], \tag{25}$$

where $\Delta = \frac{\gamma_{th}(1-\tau)}{\tau\eta\overline{\gamma}}$. And $\Delta^{\frac{m+n}{2}} K_{n-m}(2\sqrt{\Delta})$ is a monotonically increasing function with the increasing of Δ. Therefore, the throughput is improved by increasing the SNR $\overline{\gamma}$, energy conversion efficiency η, correlation coefficient ρ or decreasing the threshold γ_{th}.

Proof: See Appendix A. ∎

However, the asymptotic throughput in Proposition 1 can be further simplified. To this end, we consider two cases: namely imperfect CSI ($0 \le \rho < 1$) and perfect CSI ($\rho = 1$).

Proposition 2: The asymptotic throughput (25) can be further written as

$$R_{DL} \approx \begin{cases} R^*\Big[1 - \big(1-\rho^2\big)^{2(N-1)}\Big(\ln\Big(\frac{c\overline{\gamma}}{\gamma_{th}}\Big) - 2\gamma_{EM}\Big)\frac{\gamma_{th}}{c\overline{\gamma}}\Big], \\ \qquad\qquad 0 \le \rho < 1, \\ R^*\Big[1 - \frac{1}{\Gamma^2(N)}\Big(\ln\Big(\frac{c\overline{\gamma}}{\gamma_{th}}\Big) - 2\gamma_{EM}\Big)\Big(\frac{\gamma_{th}}{c\overline{\gamma}}\Big)^N\Big], \\ \qquad\qquad \rho = 1. \end{cases} \tag{26}$$

From (26), we directly observe that the throughput may be increased by increasing energy conversion efficiency η and SNR at the AP.

Proof: See Appendix C. ∎

Remark 1: When $\rho = 0$, namely, the user and the AP cannot obtain CSI. The average throughput then is $R^*[1 - (\ln(\frac{c\overline{\gamma}}{\gamma_{th}}) - 2\gamma_{EM})\frac{\gamma_{th}}{c\overline{\gamma}}]$. For the case of perfect CSI, the average throughput will converge to the ceiling value R^* when either the number of AP antennas or the AP transmit power increases without limit. The effect of small-scale fading between the AP and the user vanishes under this scenario. Furthermore, from Section I-D, the diversity order using OP can be obtained. For the case of imperfect CSI, the diversity order is given as $G_d = \lim_{\bar{\gamma}\to\infty} \frac{-\log P_{out}}{\log \bar{\gamma}} = 1$. In contrast, for the case of perfect CSI, the diversity order can be derived as $G_d = \lim_{\bar{\gamma}\to\infty} \frac{-\log P_{out}}{\log \bar{\gamma}} = N$.

Remark 2: Here we prove that the analytical results of [9] are special case of ours. The paper [9] studies the same system model as ours but assumes perfect CSI. Therefore, in our paper, when the correlation coefficient $\rho = 1$ (perfect CSI), $B(m,n) = 0$ for all m and n except for $B(N,N) = \frac{1}{\Gamma(N)\Gamma(N)}$. Step (a) of (61) is reduced to

$$\begin{aligned} P_{out} &= \frac{1}{\Gamma(N)}\int_0^\infty \Bigg[1 - e^{-\frac{\Delta}{y}}\sum_{l=0}^{n-1}\Big(\frac{\Delta}{y}\Big)^l \frac{1}{l!}\Bigg] y^{m-1}e^{-y}dy \\ &= 1 - 2\sum_{l=0}^{N-1}\frac{1}{l!\Gamma(N)}\Delta^{\frac{N+l}{2}} K_{N-l}\Big(2\sqrt{\Delta}\Big), \end{aligned} \tag{27}$$

which is equivalent to [9, eq. (4)].

On the other hand, [14] investigates a MIMO WPCN system with perfect CSI. The SNR in [14, eq. (8)] is a product of two independent Chi-square variables. In contrast, in our paper, the SNR (4) is the product of two weighted sums of Chi-square RVs if $\rho \neq 1$. But for $\rho = 1$, the SNR (4) is the product of two Chi-square RVs. Thus, the results in [14] for the case of $M = 1$ are equivalent to our results for $\rho = 1$.

The OP in [14, eq. (12)] is given as

$$F_\gamma(\gamma_{th}) = 1 - 2 \sum_{i=1}^{\min(N,M)} \sum_{j=|N-M|}^{(N+M)i-2i^2} \sum_{k=0}^{j} \frac{i^k d(i,j)}{k!} \left(\frac{\gamma_{th}}{D}\right)^k \times \sum_{l=1}^{\min(N,M)} \sum_{m=|N-M|}^{(N+M)l-2l^2} \frac{l^k d(l,m)}{m!} \left(\frac{il\gamma_{th}}{D}\right)^{\frac{m-k+1}{2}} \times K_{m-k+1}\left(2\sqrt{\frac{il\gamma_{th}}{D}}\right), \quad (28)$$

where N is the number of the AP antenna and M is the number of the user terminal antenna. $d(i,j) = \frac{j!}{i^{j+1}[\prod_{i=1}^{M}(M-1)!(N-i)!]}$ and $D = \frac{\eta\tau\sigma^2}{(1-\tau)Pd_1^T}$. Here, we assume the distance between the AP and the user terminal $d_1^T = 1$.

Let $M = 1$, then we have $\min(N,M) = 1$, $j = m = N-1$, $(N+M)i - 2i^2 = (N+M)l - 2l^2 = N-1$, $d(i,j) = d(l,m) = d(1,N-1) = 1$. (28) then reduces to

$$F_\gamma(\gamma_{th}) = 1 - 2\sum_{k=0}^{N-1} \frac{1}{k!\Gamma(N)} \left(\frac{\gamma_{th}}{D}\right)^{\frac{N+k}{2}} K_{N-k}\left(2\sqrt{\frac{\gamma_{th}}{D}}\right). \quad (29)$$

The OP (28), is identical to OP given in (8) in our paper, which is (27) as well, when $\rho = 1$.

In our notation, $\Delta = \frac{\gamma_{th}(1-\tau)P}{\tau\eta\sigma^2}$, which is equivalent to $\Delta = \frac{\gamma_{th}}{D}$. Therefore, (29) is identical to (27).

B. DELAY-TOLERANT TRANSMISSION MODE

1) EXACT THROUGHPUT ANALYSIS

In this mode, as mentioned before, a large delay is tolerable for decoding the stored signals together. Thus, the throughput is related to the ergodic capacity. However, the user transmits data for time fraction $(1-\tau)$ only in each cycle. Therefore, the average throughput is the product of ergodic capacity and the effective data transmit time. Thus, we find the throughput in bits/s/Hz as

$$\begin{aligned} R_{DT} &= (1-\tau)\int_0^\infty \log_2(1+z) f_{\gamma_A}(z)dz \\ &\overset{(a)}{=} (1-\tau)\sum_{n=1}^{N}\sum_{m=1}^{N} \frac{2B(m,n)}{c\overline{\gamma}} \\ &\quad \times \int_0^\infty \frac{\ln(1+z)}{\ln 2}\left(\frac{z}{c\overline{\gamma}}\right)^{\alpha(m,n)} K_{n-m}\left(2\sqrt{\frac{z}{c\overline{\gamma}}}\right)dz \\ &\overset{(b)}{=} (1-\tau)\sum_{n=1}^{N}\sum_{m=1}^{N} \frac{B(m,n)}{c\overline{\gamma}\ln 2} \\ &\quad \times G_{2,4}^{4,1}\left(\frac{1}{c\overline{\gamma}}\middle| \begin{matrix} -1, 0 \\ -1, -1, \frac{n-m}{2}+\alpha(m,n), \frac{m-n}{2}+\alpha(m,n) \end{matrix}\right), \end{aligned} \quad (30)$$

where (a) follows by the use of PDF (5); to derive (b), we express the term $\ln(1+x)$ and $x^a K_v(x)$ in Meijer G-function [42] and then use [37, eq. (7.811.1)].

Remark 3: In our paper, when channel estimation is perfect, i.e., $\rho = 1$, $\alpha(M,N) = N-1$ and $B(m,n) = 0$ for all m and n except for $B(N,N) = \frac{1}{\Gamma(N)\Gamma(N)}$. EC is then written as

$$C = \frac{(1-\tau)PG_{2,4}^{4,1}\left(\frac{(1-\tau)P}{\eta\tau\sigma^2}\middle| \begin{matrix} -1, 0 \\ -1, -1, N-1, N-1 \end{matrix}\right)}{\Gamma(N)\Gamma(N)\eta\tau\sigma^2\ln 2}. \quad (31)$$

This (31) is thus equivalent to the EC in [9, eq. (12)].

We next consider EC in [14, eq. (15)], which is given as

$$C = \frac{1}{\ln 2}\sum_{i=1}^{\min(N,M)} \sum_{j=|N-M|}^{(N+M)i-2i^2} \frac{d(i,j)}{j!} \sum_{l=1}^{\min(N,M)} \sum_{m=|N-M|}^{(N+M)l-2l^2} \frac{d(l,m)}{m!}\left(\frac{il}{D}\right) G_{2,4}^{4,1}\left(\frac{il}{D}\middle| \begin{matrix} -1, 0 \\ -1, -1, j, m \end{matrix}\right). \quad (32)$$

When $M = 1$, $\min(N,M) = 1$, $j = m = N-1$, $(N+M)i - 2i^2 = (N+M)l - 2l^2 = N-1$, $d(i,j) = d(l,m) = d(1,N-1) = 1$. Therefore, (32) is reduced to

$$C = \frac{(1-\tau)PG_{2,4}^{4,1}\left(\frac{(1-\tau)P}{\eta\tau\sigma^2}\middle| \begin{matrix} -1, 0 \\ -1, -1, N-1, N-1 \end{matrix}\right)}{\Gamma(N)\Gamma(N)\eta\tau\sigma^2\ln 2}. \quad (33)$$

Obviously, (33) is equivalent to (31).

2) ASYMPTOTIC THROUGHPUT ANALYSIS

Asymptotic throughput is derived for two regimes; namely $\overline{\gamma} \to \infty$ and $N \to \infty$ to gain insights.

Proposition 3: When $\overline{\gamma} \to \infty$, the asymptotic throughput of the delay tolerant transmission is given by

$$R_{DT} = \frac{1-\tau}{\ln 2}\left[\xi + \ln\eta\overline{\gamma} - \ln\frac{1-\tau}{\tau}\right], \quad (34)$$

where $\xi = 2\sum_{n=1}^{N} A(n)\Gamma(n)\psi(n)$ and $\psi(x)$ is the Euler psi function [37, eq. (8.360)].

Proof: Let $R_{DT} = (1-\tau)C^*$ where

$$\begin{aligned} C^* &= \mathbb{E}\big[\log_2(1+\gamma_A)\big] \\ &\approx \left[\log_2\frac{\tau\eta}{1-\tau}\overline{\gamma} + \mathbb{E}\big[\log_2(X)\big] + \mathbb{E}\big[\log_2(Y)\big]\right] \\ &= \frac{1}{\ln 2}\left[\xi + \ln\eta + \ln(\overline{\gamma}) - \ln\frac{1-\tau}{\tau}\right]. \end{aligned} \quad (35)$$

We can readily show that for RV Z, $\mathbb{E}[\log(Z)] = .\frac{d\mathbb{E}[Z^{t-1}]}{dt}|_{t=1}$. Since both X and Y have the same PDF, Z can be either X or Y. We thus find that $\mathbb{E}[Z^{t-1}] = \sum_{i=1}^{N}\frac{A(i)}{\ln 2}\Gamma(i+t-1)\psi(i+t-1)$. We differentiate this and evaluate at $t=1$, which helps to compute the two $\mathbb{E}[\log_2(\cdot)]$ terms in (35). ∎

Remark 4: From (34), for a given τ, the system throughput depends on the logarithm of $\overline{\gamma}$ at high SNR. It can be observed that increasing the value of EH time τ will let the value outside the square brackets decrease but the value inside the square brackets rises. This means the EH time

plays two conflicting roles in (34), and thus we can find an optimal value for τ to maximize the average throughput for delay-tolerant transmission mode.

Proposition 4: The optimal EH time τ^* for delay-tolerant mode at high SNR can be expressed as

$$\tau^* \approx \frac{1}{1+W\left(\eta\overline{\gamma}e^{\xi-1}\right)}, \tag{36}$$

where $W(x)$ is the Lambert W function [43].

Proof: First, we take the first-order derivative over τ of C in (34) and equate it to zero as $\frac{dC}{d\tau}=0$; We have $\xi+\ln\eta\overline{\gamma}-\frac{1}{\tau}=\ln\frac{1-\tau}{\tau}$; Then it can be written as $\eta\overline{\gamma}e^{\xi}e^{-\frac{1}{\tau}}=\frac{1-\tau}{\tau}$. Second, after some algebraic manipulations we have $\frac{1-\tau}{\tau}=W(\eta\overline{\gamma}e^{\xi-1})$. The final result is given by using $W(\cdot)$ as $\tau=\frac{1}{1+W(\eta\overline{\gamma}e^{\xi-1})}$. $W(x)$ is a monotonically increasing function for $x\geq 0$. From (36), we see that τ^* is inversely proportional to the parameters η, $\overline{\gamma}$ and ξ, where ξ is a function that depends on the number of AP antenna. ■

Proposition 5: When the number of antenna N grows without limit, the delay-tolerant throughput can be expressed as

$$\begin{aligned} R_{DT} &= (1-\tau)\mathbb{E}\left[\log_2(1+\gamma_A)\right] \\ &\approx (1-\tau)\log_2\left(1+\frac{\tau\eta}{1-\tau}\overline{\gamma}\rho^4N^2\right) \\ &\approx (1-\tau)\left[\log_2\left(\frac{\tau\eta}{1-\tau}\rho^4N^2\right)+\log_2(\overline{\gamma})\right]. \end{aligned} \tag{37}$$

Remark 5: This proposition follows from Corollary 4. The asymptotic throughput displays a logarithmic relation to the SNR, energy conversion efficiency η, the correlation coefficient and the number of AP antenna. For a given level of throughput, as $N\to\infty$, the transmit power requirements (i.e., represented by $\bar{\gamma}$) decrease. This is a beneficial trade off, resulting in less energy use. Moreover, the performance of energy and information transfer can be enhanced for long-distance transmission by adding antennas at the AP.

Remark 6: For massive MIMO systems, power scaling is an essential feature, which allows the deployment of large-scale antenna arrays to achieve the system target performance via scaling down transmit power [44], [45]. The transmit power can be scaled down as $P=\frac{\bar{P}}{N^r}$ for a fixed $\bar{P}$, and the average throughput becomes $R_{DT}\approx(1-\tau)\log_2(\frac{\tau\eta\rho^4\bar{P}}{(1-\tau)N^{2-r}})$. When $r>2$, the throughput grows without bound, which means the transmit power can be scaled down further. However, when $r<2$, the throughput converges to zero, which indicates that the transmit power has been reduced too much. When $r=2$, the throughput converges to a constant $(1-\tau)\log_2(\frac{\tau\eta}{1-\tau}\rho^4\bar{P})$.

V. AVERAGE BIT/SYMBOL ERROR RATE ANALYSIS

We next derive the error rates of our system for BPSK, BDPSK, coherent M-PSK and coherent square M-QAM. The average BER or average SER can be evaluated directly by averaging the conditional bit error rate, $P_{BER}(\cdot)$ or the conditional symbol error rate, $P_{SER}(\cdot)$ [46].

A. BPSK

1) EXACT ANALYSIS

BPSK is one of the most robust modulation schemes. Its conditional error probability is given as $P_{BER}(\gamma)=\lambda\,\mathrm{erfc}(\sqrt{\nu\gamma})$, where $\mathrm{erfc}(\cdot)$ is the complementary error function [37, eq. (8.250.1)] with $\lambda=\frac{1}{2}$ and $\nu=1$. The average BER of BPSK is given as

$$\begin{aligned} \bar{P}_{BER} &= \int_0^\infty P_{BER}(\gamma)f_{\gamma_A}(\gamma)d\gamma \\ &\overset{(a)}{=} \int_0^\infty \lambda\mathrm{erfc}\left(\sqrt{\nu\gamma}\right)\sum_{n=1}^{N}\sum_{m=1}^{N}\frac{2B(m,n)}{c\overline{\gamma}} \\ &\quad\times\left(\frac{\gamma}{c\overline{\gamma}}\right)^{\alpha(m,n)}K_{n-m}\left(2\sqrt{\frac{\gamma}{c\overline{\gamma}}}\right)d\gamma \\ &\overset{(b)}{=} \sum_{n=1}^{N}\sum_{m=1}^{N}\frac{B(m,n)\lambda}{c\overline{\gamma}\sqrt{\pi}\nu} \\ &\quad\times G_{2,3}^{2,2}\left(\frac{1}{\nu c\overline{\gamma}}\middle|\begin{matrix}0,-\frac{1}{2}\\ \frac{n-m}{2}+\alpha(m,n),\frac{m-n}{2}+\alpha(m,n),-1\end{matrix}\right), \end{aligned} \tag{38}$$

where (a) is due to submitting (5) and $P_{BER}(\gamma)$ in the equation of $\bar{P}_{BER}$; (b) is obtained by using the same integral as [46, eq. (8)] which expresses $\mathrm{erfc}(\cdot)$ in term of $G_{p,q}^{m,n}[\cdot]$ first, and then do the integral for Meijer G-function.

2) ASYMPTOTIC ANALYSIS

Since the closed-form expression (38) is complicated with the Meijer G-function, the specific relationships between the parameters and the BER are not clearly visible. However, asymptotic BER expressions are simpler.

Proposition 6: When $\bar{\gamma}\to\infty$, the asymptotic BER in this case is given as

$$\begin{aligned} \bar{P}_{BER} = \sum_{m=1}^{N}\frac{B(m,1)}{4c\overline{\gamma}}\Bigg[&(-1)^{m-2}\left(\frac{1}{c\overline{\gamma}}\right)^{m-1}e^{\frac{1}{c\overline{\gamma}}}E_i\left(-\frac{1}{c\overline{\gamma}}\right) \\ &+\sum_{k=1}^{m-1}\Gamma(k)\left(-\frac{1}{c\overline{\gamma}}\right)^{m-k-1}\Bigg]. \end{aligned} \tag{39}$$

Proof: See Appendix D. ■

Remark 7: In (39), it is seen that $\bar{P}_{BER}$ decreases when SNR $\overline{\gamma}$ increases. Although the asymptotic BER is simpler than the closed-form expression (38), it can be further simplified for two cases: imperfect CSI and perfect CSI.

Proposition 7: (39) is further simplified as

$$\bar{P}_{BER}\approx\begin{cases}\frac{\left(1-\rho^2\right)^{2(N-1)}}{4}(c\overline{\gamma})^{-1}\left[\ln\overline{\gamma}+\ln(c)-\gamma_{EM}\right], & 0\leq\rho<1,\\ \frac{\Gamma\left(N+\frac{1}{2}\right)}{2N\sqrt{\pi}\Gamma(N)(tc\overline{\gamma})^N}\Psi\left(N,1;\frac{1}{c\overline{\gamma}}\right), & \rho=1.\end{cases} \tag{40}$$

Proof: See Appendix E. ■

Remark 8: The diversity order of BPSK can be derived from (40). When CSI is imperfect ($0\leq\rho<1$), the

diversity order is $G_d = \lim_{\bar{\gamma}\to\infty} \frac{-\log \bar{P}_{BER}}{\log \bar{\gamma}} = 1$. When CSI is perfect ($\rho = 1$), the diversity order can be given as $G_d = \lim_{\bar{\gamma}\to\infty} \frac{-\log \bar{P}_{BER}}{\log \bar{\gamma}} = N$. Clearly, we see that the quality of CSI has a profound impact on the diversity order.

B. BDPSK

1) EXACT ANALYSIS

For this modulation, the conditional error probability is given by $P_{BER}(\gamma) = \lambda e^{-\nu\gamma}$. In this case, the average of $P_{BER}(\gamma)$ is simply related to the MGF of γ. So the average BER can be derived by the MGF technique [47], [48]. It is clear that the BER of BDPSK can be expressed as

$$\begin{aligned}\bar{P}_{BER} &= \lambda M_{\gamma_A}(\nu) \\ &= \sum_{n=1}^{N}\sum_{m=1}^{N} B(m,n)\lambda\left(\frac{1}{c\overline{\gamma}}\right)^{\alpha(m,n)+\frac{1}{2}}\Gamma(n)\Gamma(m) \\ &\quad \times e^{\frac{1}{2\nu c\overline{\gamma}}}\nu^{-\frac{1}{2}-\alpha(m,n)}W_{-\frac{1}{2}-\alpha(m,n),\frac{n-m}{2}}\left(\frac{1}{\nu c\overline{\gamma}}\right).\end{aligned} \tag{41}$$

For BDPSK, the parameter values are $\lambda = \frac{1}{2}$ and $\nu = 1$. Although this result is exact, simpler yet accurate results are possible with the use of asymptotic MGF.

2) ASYMPTOTIC ANALYSIS

To this end, we can use Corollary 2 to obtain the asymptotic performance of BDPSK. Thus, the asymptotic BER ($\bar{\gamma} \to \infty$) is given by

$$\begin{aligned}\bar{P}_{BER} &= \lambda M^{asy}_{\gamma_A}(\nu) \\ &= \sum_{m=1}^{N}\frac{B(m,1)}{\nu c\overline{\gamma}} \\ &\quad \times \left[\sum_{k=1}^{m-1}\Gamma(k)\left(-\frac{1}{\nu c\overline{\gamma}}\right)^{m-1-k}\right. \\ &\qquad \left. + (-1)^{m-2}e^{\frac{1}{\nu c\overline{\gamma}}}\left(\frac{1}{\nu c\overline{\gamma}}\right)^{m-1}E_i\left(-\frac{1}{\nu c\overline{\gamma}}\right)\right].\end{aligned} \tag{42}$$

However, even further simplification is possible. By using Corollary 3, thus, asymptotic $\bar{P}_{BER}$ is obtained as follows;

$$\bar{P}_{BER} \approx \begin{cases} \lambda\left(1-\rho^2\right)^{2(N-1)}(c\nu\overline{\gamma})^{-1} \\ \cdot\left[\ln\overline{\gamma} + \ln c\nu - \gamma_{EM}\right], & 0 \le \rho < 1, \\ \frac{\lambda(\nu c\overline{\gamma})^{-N}}{\Gamma(N)}\Psi\left(N, 1; \frac{1}{\nu c\overline{\gamma}}\right), & \rho = 1. \end{cases} \tag{43}$$

Remark 9: According to (43), when $0 \le \rho < 1$ the diversity order can be derived as $G_d = \lim_{\bar{\gamma}\to\infty} \frac{-\log \bar{P}_{BER}}{\log \bar{\gamma}} = 1$. When the CSI is perfect, the diversity order is $G_d = \lim_{\bar{\gamma}\to\infty} \frac{-\log \bar{P}_{BER}}{\log \bar{\gamma}} = N$. Thus, we see that the diversity order collapses when the quality of CSI is less than perfect.

C. FOR COHERENT M-PSK

M-PSK modulation is widely used in advanced wireless networks such as LTE, WiMAX and others. For a given symbol rate, the information rate of M-PSK is significantly higher than that of BPSK. However, it needs more transmit power to keep the same error rates as BPSK.

1) EXACT ANALYSIS

The conditional SER for coherent M-PSK signals is given by [49]

$$P_{SER}(\gamma) = a\int_0^{\Lambda} e^{-b(\theta)\gamma}d\theta,$$

where $a = \frac{1}{\pi}$, $\Lambda = \frac{(M-1)\pi}{M}$, $b(\theta) = \frac{g_{PSK}}{\sin^2(\theta)}$ and $g_{PSK} = \sin^2(\frac{\pi}{M})$. Since the SER expression is an integral of the exponential function, the expected value of this expression directly relates to the MGF.

Thus, the average SER, $\bar{P}_{SER}$, can be derived as

$$\begin{aligned}\bar{P}_{SER} &= a\int_0^{\Lambda} M_{\gamma_A}(b(\theta))d\theta \\ &= \sum_{n=1}^{N}\sum_{m=1}^{N} aB(m,n)\left(\frac{1}{c\overline{\gamma}}\right)^{\alpha(m,n)+\frac{1}{2}}\Gamma(n)\Gamma(m) \\ &\quad \times \int_0^{\Lambda} e^{\frac{1}{2b(\theta)c\overline{\gamma}}}b(\theta)^{-\frac{1}{2}-\alpha(m,n)}W_{-\frac{1}{2}-\alpha(m,n),\frac{n-m}{2}}\left(\frac{1}{b(\theta)c\overline{\gamma}}\right)d\theta,\end{aligned} \tag{44}$$

where $\bar{P}_{SER}$ is obtained by Lemma 2. The finite integrals in (44) can be evaluated by mathematical software packages.

2) ASYMPTOTIC ANALYSIS

We see that (44) has the Whittaker function, a complicated function. Thus, the relations between the parameters and the SER are not immediately evident. To alleviate this, similar to the BDPSK case, we derive the asymptotic results via Corollary 3 (Section III)

$$\begin{aligned}\bar{P}_{SER} &= a\int_0^{\Lambda} M^{asy}_{\gamma_A}(b(\theta))d\theta \\ &= \sum_{m=1}^{N}\int_0^{\Lambda}\frac{B(m,1)}{b(\theta)c\overline{\gamma}} \\ &\quad \times \left[\sum_{k=1}^{m-1}\Gamma(k)\left(-\frac{1}{b(\theta)c\overline{\gamma}}\right)^{m-1-k}\right. \\ &\qquad \left. + (-1)^{m-2}e^{\frac{1}{b(\theta)c\overline{\gamma}}}\left(\frac{1}{b(\theta)c\overline{\gamma}}\right)^{m-1}E_i\left(-\frac{1}{b(\theta)c\overline{\gamma}}\right)\right]d\theta,\end{aligned} \tag{45}$$

where, the finite integrals in (45) can be evaluated by software.

We can simplify it further for imperfect CSI case ($0 \le \rho < 1$) and perfect CSI case ($\rho = 1$), respectively as

$$\begin{aligned}\bar{P}_{SER} &\approx a\int_0^{\Lambda}\left(1-\rho^2\right)^{2(N-1)}(cb(\theta)\overline{\gamma})^{-1} \\ &\quad \times \left[\ln\overline{\gamma} + \ln(cb(\theta)) - \gamma_{EM}\right]d\theta\end{aligned} \tag{46}$$

and

$$\bar{P}_{SER} \approx a \int_0^{\Lambda} \frac{\lambda (b(\theta) c\overline{\gamma})^{-N}}{\Gamma(N)} \Psi\left(N, 1; \frac{1}{b(\theta) c\overline{\gamma}}\right) d\theta. \quad (47)$$

D. M-QAM

M-QAM is widely used in digital communication networks. These include optical fiber networks, digital subscriber lines, IEEE 802.11, orthogonal frequency division mulitplexing (OFDM) based networks and more. By increasing constellation size M, it is possible achieve arbitrarily high spectral efficiencies.

1) EXACT ANALYSIS

The conditional SER for coherent square M-QAM signals is given by [50], [49]

$$P_{SER}(\gamma) = \frac{4q}{\pi} \int_0^{\frac{\pi}{2}} e^{-h(\theta)\gamma} d\theta - \frac{4q^2}{\pi} \int_0^{\frac{\pi}{4}} e^{-h(\theta)\gamma} d\theta, \quad (48)$$

where $q = 1 - \frac{1}{\sqrt{M}}$, $h(\theta) = \frac{g_{QAM}}{\sin^2(\theta)}$ and $g_{QAM} = \frac{3}{2(M-1)}$. Then, SER of M-QAM can be derived as follow

$$\begin{aligned} \bar{P}_{SER} &= \int_0^{\infty} P_e(\gamma) f_{\gamma_A}(\gamma) d\gamma \\ &= I_1 - I_2, \end{aligned} \quad (49)$$

where I_1 and I_2 can be written as

$$\begin{aligned} I_1 &= \frac{4q}{\pi} \int_0^{\frac{\pi}{2}} M_{\gamma_A}(h(\theta)) d\theta \\ &= \frac{4q}{\pi} \sum_{n=1}^{N} \sum_{m=1}^{N} B(m,n) \left(\frac{1}{c\overline{\gamma}}\right)^{\alpha(m,n)+\frac{1}{2}} \Gamma(n)\Gamma(m) \\ &\quad \times \int_0^{\frac{\pi}{2}} e^{\frac{1}{2h(\theta)c\overline{\gamma}}} h(\theta)^{-\frac{1}{2}-\alpha(m,n)} W_{-\frac{1}{2}-\alpha(m,n), \frac{n-m}{2}}\left(\frac{1}{h(\theta)c\overline{\gamma}}\right) d\theta \end{aligned} \quad (50)$$

and

$$\begin{aligned} I_2 &= \frac{4q^2}{\pi} \int_0^{\frac{\pi}{4}} M_{\gamma_A}(h(\theta)) d\theta \\ &= \frac{4q^2}{\pi} \sum_{n=1}^{N} \sum_{m=1}^{N} B(m,n) \left(\frac{1}{c\overline{\gamma}}\right)^{\alpha(m,n)+\frac{1}{2}} \Gamma(n)\Gamma(m) \\ &\quad \times \int_0^{\frac{\pi}{4}} e^{\frac{1}{2h(\theta)c\overline{\gamma}}} h(\theta)^{-\frac{1}{2}-\alpha(m,n)} W_{-\frac{1}{2}-\alpha(m,n), \frac{n-m}{2}}\left(\frac{1}{h(\theta)c\overline{\gamma}}\right) d\theta. \end{aligned} \quad (51)$$

The finite integrals in (50) and (51) can be evaluated by software such as MATLAB.

2) ASYMPTOTIC ANALYSIS

We can also find an asymptotic expression for (49). Similar to the case of BDPSK, we obtain the asymptotic result by using Corollary 2.

$$\bar{P}_{SER} \approx P_1 - P_2, \quad (52)$$

where

$$\begin{aligned} P_1 &= \frac{4q}{\pi} \int_0^{\frac{\pi}{2}} M_{\gamma_A}^{asy}(h(\theta)) d\theta \\ &= \sum_{m=1}^{N} \frac{4q}{\pi} \int_0^{\frac{\pi}{2}} \frac{B(m,1)}{h(\theta)c\overline{\gamma}} \\ &\quad \times \left[\sum_{k=1}^{m-1} \Gamma(k) \left(-\frac{1}{h(\theta)c\overline{\gamma}}\right)^{m-1-k} \right. \\ &\quad \left. + (-1)^{m-2} e^{\frac{1}{h(\theta)c\overline{\gamma}}} \left(\frac{1}{h(\theta)c\overline{\gamma}}\right)^{m-1} E_i\left(-\frac{1}{h(\theta)c\overline{\gamma}}\right) \right] d\theta \end{aligned} \quad (53)$$

and

$$\begin{aligned} P_2 &= \frac{4q^2}{\pi} \int_0^{\frac{\pi}{4}} M_{\gamma_A}^{asy}(h(\theta)) d\theta \\ &= \sum_{m=1}^{N} \frac{4q^2}{\pi} \int_0^{\frac{\pi}{4}} \frac{B(m,1)}{h(\theta)c\overline{\gamma}} \\ &\quad \times \left[\sum_{k=1}^{m-1} \Gamma(k) \left(-\frac{1}{h(\theta)c\overline{\gamma}}\right)^{m-1-k} \right. \\ &\quad \left. + (-1)^{m-2} e^{\frac{1}{h(\theta)c\overline{\gamma}}} \left(\frac{1}{h(\theta)c\overline{\gamma}}\right)^{m-1} E_i\left(-\frac{1}{h(\theta)c\overline{\gamma}}\right) \right] d\theta, \end{aligned} \quad (54)$$

where the finite integrals in (53) and (54) can be readily evaluated by software such as MATLAB.

Using Corollary 3, for the imperfect case, when $0 \le \rho < 1$ we can obtain

$$\begin{aligned} P_1 &\approx \frac{4q}{\pi} \int_0^{\frac{\pi}{2}} \left(1-\rho^2\right)^{2(N-1)} (ch(\theta)\overline{\gamma})^{-1} \\ &\quad \times \left[\ln \overline{\gamma} + \ln(ch(\theta)) - \gamma_{EM}\right] d\theta \end{aligned} \quad (55)$$

and

$$\begin{aligned} P_2 &\approx \frac{4q^2}{\pi} \int_0^{\frac{\pi}{4}} \left(1-\rho^2\right)^{2(N-1)} (ch(\theta)\overline{\gamma})^{-1} \\ &\quad \times \left[\ln \overline{\gamma} + \ln(ch(\theta)) - \gamma_{EM}\right] d\theta. \end{aligned} \quad (56)$$

For the perfect CSI case, where $\rho = 1$, we have

$$P_1 \approx \frac{4q}{\pi} \int_0^{\frac{\pi}{2}} \frac{(h(\theta)c\overline{\gamma})^{-N}}{\Gamma(N)} \Psi\left(N, 1; \frac{1}{h(\theta)c\overline{\gamma}}\right) d\theta \quad (57)$$

and

$$P_2 \approx \frac{4q^2}{\pi} \int_0^{\frac{\pi}{4}} \frac{(h(\theta)c\overline{\gamma})^{-N}}{\Gamma(N)} \Psi\left(N, 1; \frac{1}{h(\theta)c\overline{\gamma}}\right) d\theta. \quad (58)$$

Remark 10: For BDPSK, M-PSK and M-QAM, the exact expressions are derived based on Lemma III.B, and the asymptotic results are based on Corollary 2 and Corollary 3 (Section III). For the imperfect CSI case, where $0 \le \rho < 1$, it can be seen from (40), (43), (46), (55) and (56) that when the value of the product of $c\overline{\gamma}$ increases, the value of average BER/SER will converge to zero, which means either the energy conversion efficiency at the user or the AP transmit power rises, the BER/SER can be improved. For the perfect CSI case ($\rho = 1$), $\bar{P}_{BER}$ contains a confluent hypergeometric function and the impact of the parameters is not as explicit as the imperfect CSI case.

TABLE 1. Simulation parameters.

Notation	Parameter	Value
T	Block duration	1
σ^2	Noise variance	0 dBm
$\bar{\gamma}$	unfaded SNR	
ρ	correlation	

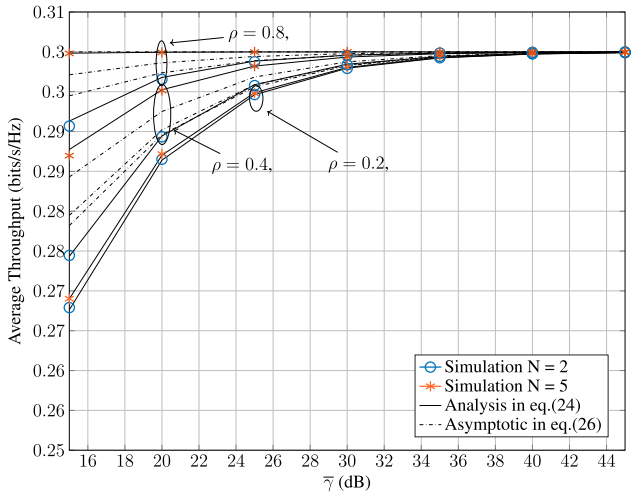

FIGURE 2. Delay-limited throughput mode versus average SNR ($\overline{\gamma}$) for $\tau = 0.4$, $\eta = 0.6$ and $R = 0.5$.

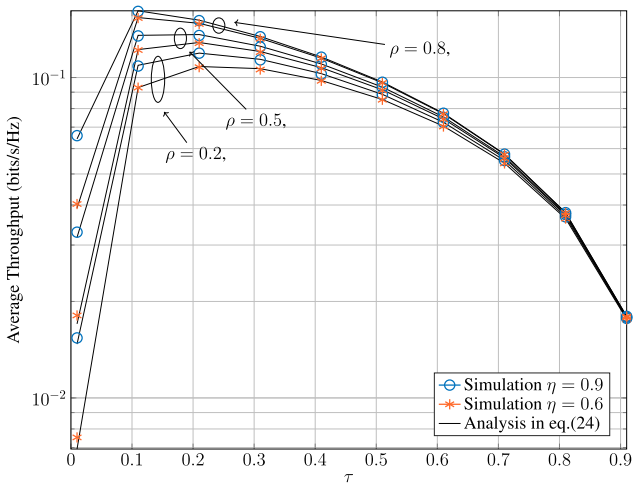

FIGURE 3. Delay-limited throughput versus EH time (τ) for $N = 3$ and $P = 10$ dBm.

VI. NUMERICAL AND SIMULATION RESULTS

This section provides Monte-Carlo simulations to validate analytical results and to evaluate the impacts of the key parameters, which are given in Table 1.

A. DELAY-LIMITED MODE

Fig. 2 plots the delay-limited throughput versus the average SNR with different numbers of AP antennas and the correlation coefficient ρ. As expected, when the transmit power or the number of AP antennas is increased, the average throughput improves. The simple reason is that more harvested energy is achieved as a result of higher energy beamforming gain and the AP transmit power. The throughput is also influenced by the quality of the CSI (e.g., correlation coefficient). When $\rho \approx 1$, the system has perfect CSI without noisy estimates. If $\rho \approx 0$, the poor performance results in poor throughput. The dotted lines represent the asymptotic throughput for $\overline{\gamma} \to \infty$ in (26), which improves when ρ and the AP transmit power increase. When $\overline{\gamma}$ is large, all the curves converge to 0.3, which validates our analytical result that $R_{DL} = R^*$ as $\overline{\gamma} \to \infty$.

Fig. 3 plots the simulated and exact outage probability versus EH time τ with different correlation coefficients (ρ) and energy conversion efficiencies (η). We can observe that the throughput improves with increasing ρ. The figure also shows the relation between average throughput and energy conversion efficiency. Obviously, higher η helps the user harvest more energy in the DL, so the user has more energy for UL data transmission. The curves are concave and they increase first and then decrease as the EH time increases. It is observed that the peak for the $\rho = 0.8$ curve is at $\tau = 0.1$, while the peaks for curves $\rho = 0.5$ and $\rho = 0.2$ are at $\tau = 0.2$. Thus, the optimal EH time is sensitive to the quality of channel estimations.

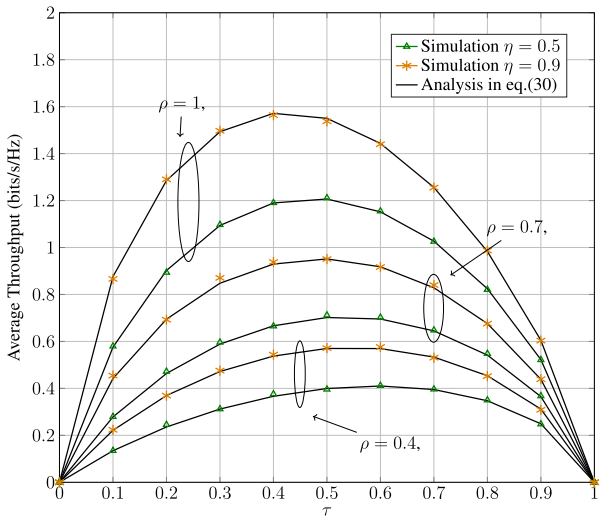

FIGURE 4. Delay-tolerant throughput versus EH time τ for $P = 1$ dBm and $N = 3$.

B. DELAY-TOLERANT MODE

Fig. 4 plots the delay-tolerant throughput versus EH time τ for several energy conversion efficiencies (η) and correlation coefficients (ρ). The figure shows a peak for each curve. This optimal EH time, τ^*, balances EH time, τ, and data transmission time, $(1 - \tau)$, perfectly. This coincides with our analytical results (30) and (36). Note that $\rho \approx 1$ is for perfect CSI and $\rho \approx 0$ is for totally noisy CSI. Thus, we can observe that larger ρ and η increase the throughput. Finally, we note that the simulation points (e.g., markers) lie exactly on the solid curves, which are the analytical results. Thus, this confirms that the derived theoretical results match

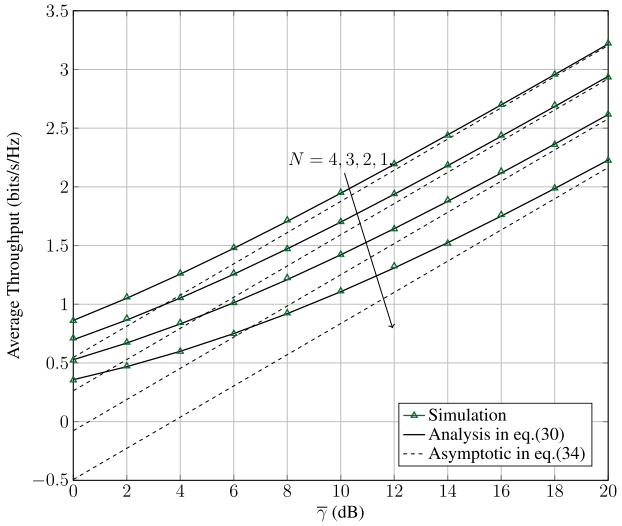

FIGURE 5. Delay-tolerant throughput versus $\overline{\gamma}$ for $\eta = 0.9$, $\tau = 0.6$ and $\rho = 0.6$.

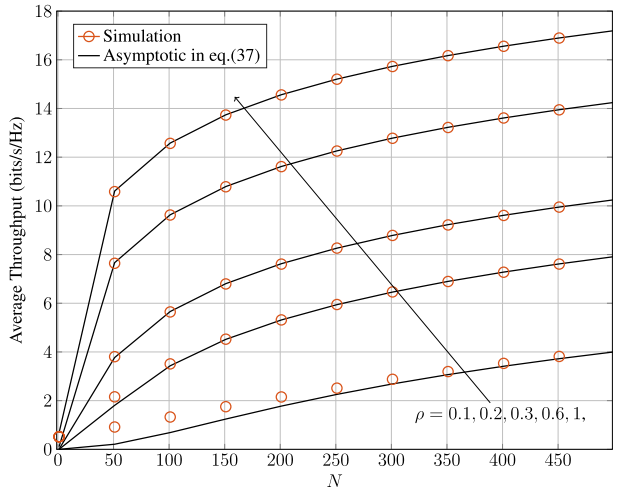

FIGURE 6. Delay-tolerant throughput versus N for $\eta = 0.9$ and $\tau = 0.4$.

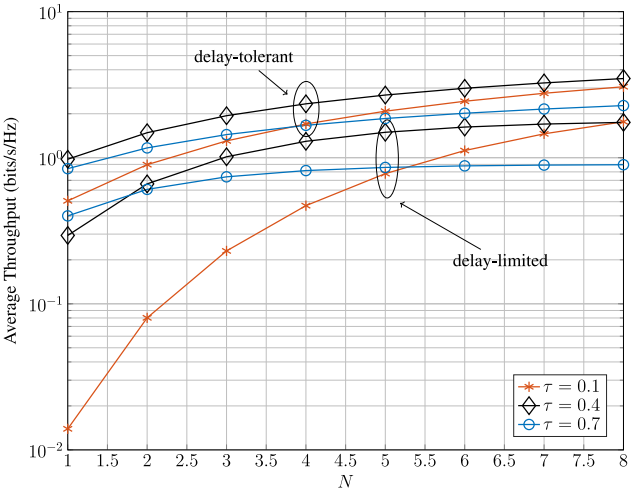

FIGURE 7. Average throughput versus the number of AP antennas for both delay-limited delay-tolerant modes with different EH time τ, $P = 10$ dBm, and $\rho = 0.7$.

with the simulations. This assures some confidence about the validity of the theoretical results.

Fig. 5 plots the delay-tolerant throughput versus the AP transmit power with different numbers of AP antennas. Increasing both the transmit power and the number of antennas builds up the ergodic capacity. As well, the simulation result matches the analytical result in (30). Although the asymptotic curves (34) and the analytical curves (30) diverge for small values of the SNR ($\overline{\gamma}$), they converge as $\overline{\gamma}$ increases. Hence, the asymptotic expression is useful to correctly predict the characteristic of the delay-tolerant throughput performance in high SNR region.

Fig. 6 plots the delay-tolerant throughput versus the number of AP antennas, N. The solid lines and the circle markers represent the asymptotic analysis and simulations, respectively. The slopes of curves are large when N is small, but increasing N flattens out the curves. The asymptotic results converge to the simulations when either the number of antennas increase or ρ increase. When $\rho \approx 1$, i.e., noise-free estimates, the simulation and asymptotic results coincide even for small N. However, with more noisy estimates, more antennas are needed to obtain a convergence between asymptotic and simulation results. Finally, as before, increasing ρ improves the throughput.

Fig. 7 shows average throughput of delay-limited and delay-tolerant modes versus the number of AP antennas, N and different values of the EH time τ. The throughput of the delay-tolerant mode increases with more AP antennas, and the slope of the curves gradually decreases. On the other hand, the throughput curves of the delay-limited mode first increases and then reach a ceiling when N increases. This behaviour can be anticipated from (24) because the average throughput of the delay-limited mode is bounded by R^*. Moreover, it can be observed that the impact of τ for both throughput performances is unclear.

C. BER

Fig. 8 plots the BERs of BPSK in (38) and BDPSK in (41) versus EH time τ with different numbers of AP antennas. Solid lines represent the analytical results, while the markers (triangle and star) represent the simulation points. Thus, we clearly see a tight fit between simulation and the analytical results. BPSK has better performance than BDPSK for same parameters. It is observed that the deployment of more AP antennas improves the BER of both BPSK and BDPSK. Unlike the average throughput, where certain τ results in the peak, the BER decreases when τ increases. We thus observe that the minimum BER is obtained when $\tau = 0.9$. This trend can be clearly seen from the asymptotic results (40) and (43). Of course, such large values of τ are not helpful in terms of throughput maximization.

Fig. 9 plots the average BER of BDPSK versus SNR for different EH conversion efficiencies ($\eta = 0.6, 0.8$) and EH times ($\tau = 0.2, 0.4, 0.8$). We see that the asymptotic results (dashed lines) approach the exact (solid lines) and

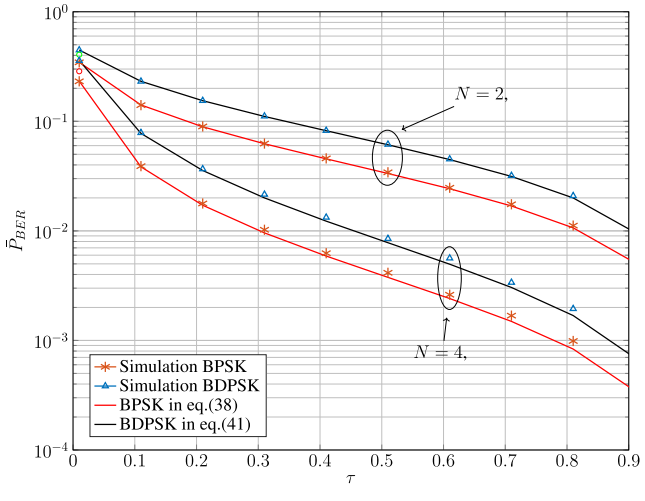

FIGURE 8. $\bar{P}_{BER}$ versus τ for $\rho = 0.8$, $\eta = 0.9$, $\nu = 1$ and $\lambda = 0.5$.

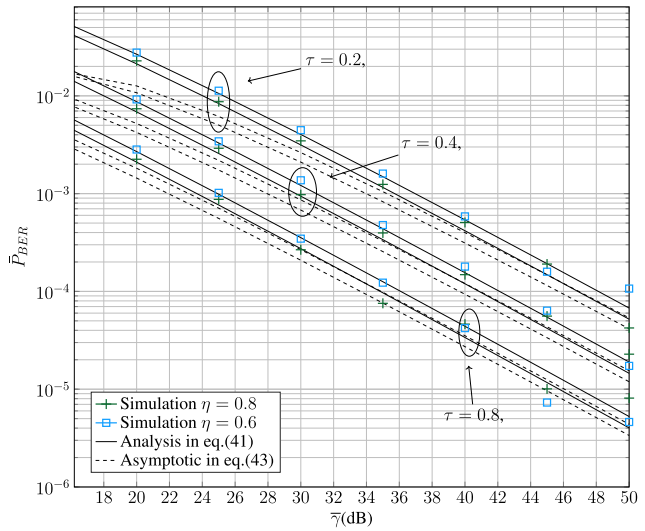

FIGURE 9. $\bar{P}_{BER}$ of BDPSK versus $\bar{\gamma}$ for $N = 4$, $\rho = 0.5$, $\nu = 1$ and $\lambda = 0.5$.

simulation ones (markers) when SNR increases. As well, increasing SNR improves the BER performance. The BER decreases when the EH conversion efficiency or the EH time increases. It is observed that gaps between asymptotic and analysis depends on the EH time. τ. It also can be observed that increasing EH time clearly improves the BER performance.

Fig. 10 plots analytical, simulated and asymptotic BERs of BPSK versus SNR. The number of AP antennas (N) is assumed as either 2 or 4, and the correlation coefficient (ρ) is 0.2, 0.4 or 0.8. Similar to the BDPSK case, increasing SNR improves the BER performance. In addition, Fig. 10 shows that either adding more antennas at the AP or increasing the correlation coefficient can decrease BER. We can also see the analytical (solid lines) and asymptotic (dashed lines) results diverge for ($N = 4$, $\rho = 0.8$), but when N decreases, the gaps between analytical and asymptotic results are reduced quickly.

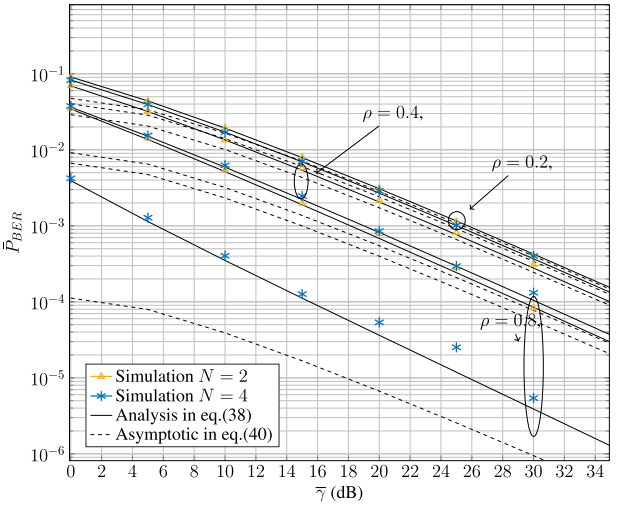

FIGURE 10. $\bar{P}_{BER}$ of BPSK versus $\bar{\gamma}$ for $\tau = 0.8$, $\eta = 0.5$, $\nu = 1$ and $\lambda = 0.5$.

VII. CONCLUSION

Although there has been a flurry of works on WPCNs, the impact of channel estimation errors on their performance has received scant attention. Thus, this paper investigated this topic in detail. Specifically, we analyzed the distributions of the received SNR, the average throughput of delay-tolerant, delay-limit modes, and the BER/SER performances. Exact closed-form expressions as well as the high-SNR asymptotic results were derived. The correctness and effectiveness of these theoretical analysis were verified by Monte-Carlo simulation results. Our results show that in the high SNR region, the performance of one transmit and receive antenna coincides with that of multiple antennas at the AP. Due to energy beamforming at the DL, when the AP transmit power is large enough, the energy user harvests from one path is sufficient for the UL information transmission. Numerical results showed that optimal EH times for delay-tolerant and delay-limit modes are different.

Our main findings from the derivations and the numerical results can be summarized as follows:

1) Unsurprisingly, the throughput and BER/SER performances can be improved by increasing the transmit power P, the number of antennas at the AP, correlation coefficient and EH conversion efficiency.
2) The optimal EH time fraction τ which maximizes the EH and data transmission rate can be derived for the delay-tolerant mode.
3) In the conventional analysis of non-EH wireless [33], [51], the asymptotic performance (e.g., BER, SER and outage) can be expressed in terms of diversity gain and coding gain (see (1)). But we have shown that this breaks down in the case of EH links. Instead, most asymptotic expressions tend to be of the form $\frac{\ln(\bar{\gamma})+c}{\bar{\gamma}^d}$ where c and d are some constants.

4) When the number of AP antennas becomes very large, the effect of small-scale fading vanishes. This is the well-known channel hardening effect in the massive MIMO literature.

A. FUTURE DIRECTIONS

Although the effect of imperfect CSI on a WPCN has been the focus of this paper, several interesting future directions suggest by themselves. Firstly, we assumed a linear EH model where the EH output power increases linearly and unbounded with the input RF signal power. However, practical EH circuits display highly nonlinear characteristics, exhibiting saturation with high input powers. Thus, nonlinear EH models are of interest [52], which may thus be considered for the extension of our results in this paper. Secondly, our work may also be extended for non-orthogonal multiple access (NOMA) assisted WPCNs. For example, the exact and asymptotic performances of imperfect CSI can be evaluated in NOMA WPCNs. Thirdly, we have assumed independent fading across the multiple AP antennas. Although this assumption roughly holds for the most practical operating conditions, correlated fading can occur sometimes. So analytical tools for the correlated fading case are important to be developed. Finally, our work can also be extended to MIMO systems.

APPENDIX A
PROOF OF PROPOSITION 1

To develop this analysis, we must go back to the definition of γ_A. By using it and revisiting (23), we can exactly express the delay-limited throughput as

$$P_{out} = \Pr\left(XY < \frac{(1-\tau)\gamma_{th}}{\tau\eta\overline{\gamma}}\right). \tag{59}$$

As mentioned before, to find the asymptotics of the outage, we need the series expansion of the PDF of XY, similar to (1). We then have to consider the behaviour of $K_n(x)$ as $x \to 0$. But the expansion of this function near $x = 0$ has logarithmic terms and negative powers of x [37]. Due to this reason, the classical approach is not viable. Alternatively, we use the two-step process, which was earlier used to derived the asymptotic MGF. The first step is to average over X while keeping Y constant. Since the PDF of X is a weight sum (6), the outage for conditioned on Y, $P_{out}\,|_Y$, may then be written as

$$P_{out}\,|_Y = \sum_{n=1}^{N} A(n)\Gamma(n)\left[1 - e^{-\frac{\Delta}{y}}\sum_{l=0}^{n-1}\left(\frac{\Delta}{y}\right)^l\frac{1}{l!}\right]. \tag{60}$$

The second step is to average the conditional outage over the PDF of Y when $\overline{\gamma} \to \infty$. This can be done as follows:

$$\begin{aligned} P_{out} &= \int_0^{\infty} P_{out}\,|_Y f_Y(y)dy \\ &\overset{(b)}{=} \sum_{n=1}^{N}\sum_{m=1}^{N} B(m,n)\Gamma(n) \\ &\quad\times \int_0^{\infty}\underbrace{\left[1 - e^{-\frac{\Delta}{y}}\sum_{l=0}^{n-1}\left(\frac{\Delta}{y}\right)^l\frac{1}{l!}\right]}_{I} y^{m-1}e^{-y}dy \\ &\overset{(c)}{=} 2\sum_{n=1}^{N}\sum_{m=1}^{N} B(m,n)\Delta^{\frac{m+n}{2}}K_{n-m}\left(2\sqrt{\Delta}\right), \end{aligned} \tag{61}$$

where Step (a) is obtained by substituting the PDF of Y in (60); The proof of Step (b) is obtained in the Appendix B.

Therefore, the average throughput can be written as (25).

APPENDIX B
APPROXIMATION FOR OP

Here, we derive the approximation expression of the term in Step (a) in (61). Recall that $\Delta = \frac{\gamma_{th}(1-\tau)}{\tau\eta\overline{\gamma}}$, so when $\overline{\gamma} \to \infty$, $\Delta \to 0$ and I can be approximated as

$$\begin{aligned} I &= 1 - e^{-\frac{\Delta}{y}}\sum_{l=0}^{n-1}\left(\frac{\Delta}{y}\right)^l\frac{1}{l!} \\ &\overset{(a)}{=} e^{-\frac{\Delta}{y}}\left[e^{\frac{\Delta}{y}} - \sum_{l=0}^{n-1}\left(\frac{\Delta}{y}\right)^l\frac{1}{l!}\right] \\ &\overset{(b)}{=} e^{-\frac{\Delta}{y}}\sum_{l=n}^{\infty}\left(\frac{\Delta}{y}\right)^l\frac{1}{l!} \\ &\overset{(c)}{\approx} e^{-\frac{\Delta}{y}}\left(\frac{\Delta}{y}\right)^n\frac{1}{n!}, \end{aligned} \tag{62}$$

where, (a) follows readily; (b) is due to Taylor expansion $e^{\frac{\Delta}{y}} = \sum_{l=0}^{\infty}(\frac{\Delta}{y})^l\frac{1}{l!}$; When $\Delta \to 0$, the terms for $l \geq n+1$ are much smaller than the $l = n$-th term, so we can ignore all the terms for which $l \geq n+1$. Therefore, we obtain (c).

The integral in Step (a) in (61) can be approximated as

$$\begin{aligned} &\int_0^{\infty}\left[1 - e^{-\frac{\Delta}{y}}\sum_{l=0}^{n-1}\left(\frac{\Delta}{y}\right)^l\frac{1}{l!}\right]y^{m-1}e^{-y}dy \\ &\quad\approx \Delta^n\frac{1}{n!}\int_0^{\infty} e^{-\frac{\Delta}{y}-y}y^{m-n-1}dy \\ &\quad= \Delta^{\frac{m+n}{2}}K_{n-m}\left(2\sqrt{\Delta}\right), \end{aligned} \tag{63}$$

which is obtained by using [37, eq. (3.471.9)]. By substituting this in (61), we obtain the final result.

APPENDIX C
PROOF OF PROPOSITION 2

For the imperfect CSI case, where $0 \leq \rho < 1$, when SNR is large, the first term of (61) will be the dominant term, and thus the whole sum in (61) can be approximated by it. For the term with $m = 1$ and $n = 1$, equation (b) in (61) can be written as

$$\begin{aligned} P_{out} &\approx 2\left(1-\rho^2\right)^{2(N-1)}\Delta K_0\left(2\sqrt{\Delta}\right) \\ &\overset{(a)}{=} 2\left(1-\rho^2\right)^{2(N-1)}\Delta\left(-\frac{1}{2}\ln\Delta - \gamma_{EM}\right) + O\left(\Delta^2\right) \\ &\overset{(b)}{=} \left(1-\rho^2\right)^{2(N-1)}\left(\ln\left(\frac{c\overline{\gamma}}{\gamma_{th}}\right) - 2\gamma_{EM}\right)\frac{\gamma_{th}}{c\overline{\gamma}} \end{aligned} \tag{64}$$

To obtain (a), we note that near $x = 0$, the Bessel function can be expanded as $K_0(2\sqrt{x}) = -\frac{1}{2}\ln x - \gamma_{EM} + O(x)$. We can use this expansion because as $\overline{\gamma} \to \infty$, $\Delta \to 0$. (b) represents the equation in $\overline{\gamma}$.

Therefore, the average throughput is expressed as

$$R_{DL} = R^*\left[1 - \left(1-\rho^2\right)^{2(N-1)}\left(\ln\left(\frac{c\overline{\gamma}}{\gamma_{th}}\right) - 2\gamma_{EM}\right)\frac{\gamma_{th}}{c\overline{\gamma}}\right]. \tag{65}$$

For the perfect CSI case, when $\rho = 1$, $B(m, n)$ exists only when $m = N$ and $n = N$, so (61) can be written as

$$\begin{aligned} P_{out} &\approx \frac{2}{\Gamma^2(N)}\Delta^N K_0\left(2\sqrt{\Delta}\right) \\ &\overset{(a)}{=} \frac{2}{\Gamma^2(N)}\Delta^N\left(-\frac{1}{2}\ln\Delta - \gamma_{EM}\right) + O\left(\Delta^{N+1}\right) \\ &\overset{(b)}{\approx} \frac{1}{\Gamma^2(N)}\left(\ln\left(\frac{c\overline{\gamma}}{\gamma_{th}}\right) - 2\gamma_{EM}\right)\left(\frac{\gamma_{th}}{c\overline{\gamma}}\right)^N. \end{aligned} \tag{66}$$

The proof of this is very similar to that of (64) and therefore the details are omitted. Thus, the average throughput can be expressed as

$$R_{DL} = R^*\left[1 - \frac{1}{\Gamma^2(N)}\left(\ln\left(\frac{c\overline{\gamma}}{\gamma_{th}}\right) - 2\gamma_{EM}\right)\left(\frac{\gamma_{th}}{c\overline{\gamma}}\right)^N\right]. \tag{67}$$

APPENDIX D
PROOF OF PROPOSITION 6

First, we express the BER by using the Q function, and then take the expectation of the BER. Therefore, the average BER of BPSK can be expressed as

$$\bar{P}_{BER} = \mathbb{E}\left[Q\left(\sqrt{2c\overline{\gamma}XY}\right)\right], \tag{68}$$

where the Gaussian Q-function is given by $Q(x) = \frac{1}{\sqrt{2\pi}}\int_x^\infty e^{-t^2/2}dt = \frac{1}{2\sqrt{\pi}}\Gamma(\frac{1}{2}, \frac{x^2}{2})$. Therefore, (68) can be rewritten as

$$\bar{P}_{BER} = \mathbb{E}\left[\frac{1}{2\sqrt{\pi}}\Gamma\left(\frac{1}{2}, c\overline{\gamma}XY\right)\right]. \tag{69}$$

Next, we use the following two steps to find the asymptotic BER.

In Step 1, we average (69) over X while keeping Y constant. Since the PDF of X is a weighted sum of exponential terms (6), the BER conditional on Y may be written as

$$\begin{aligned} \bar{P}_{BER|Y} &= \sum_{n=1}^{N}\frac{A(n)}{2\sqrt{\pi}}\int_0^\infty \Gamma\left(\frac{1}{2}, c\overline{\gamma}xy\right)x^{n-1}e^{-x}dx \\ &\overset{(a)}{=} \sum_{n=1}^{N}\frac{A(n)}{2n\sqrt{\pi}}\frac{\sqrt{c\overline{\gamma}y}\Gamma\left(n+\frac{1}{2}\right)}{(1+c\overline{\gamma}y)^{n+\frac{1}{2}}} \\ &\quad \times {}_2F_1\left(1, n+\frac{1}{2}; n+1; \frac{1}{1+c\overline{\gamma}y}\right) \\ &\overset{(b)}{\approx} \sum_{n=1}^{N}\frac{A(n)}{2n\sqrt{\pi}}\frac{\Gamma\left(n+\frac{1}{2}\right)}{(1+c\overline{\gamma}y)^n} \\ &\overset{(c)}{\approx} \frac{1}{4}\frac{1}{1+c\overline{\gamma}y}. \end{aligned} \tag{70}$$

Step (a) is obtained by calculating the integral part of the conditional BER given by Y and using [37, eq. (6.455.1)]; ${}_2F_1(a, b; c; z)$ is hypergeometric function [37, eq. (9.10)] which can be written by the power series when $|z| < 1$. ${}_2F_1(a, b; c; z) = \sum_{k=0}^{\infty}\frac{(a)_k(b)_k}{(c)_k}\frac{z^k}{k!}$, where if $k = 0$, $(q)_k = 1$ and if $k > 0$, $(q)_k = q(q+1)\cdots(q+k-1)$. In step (b), since $\overline{\gamma} \to \infty$, the parts for which $n \geq 2$ is small compared to those with $n = 1$, so the parts for $n \geq 0$ can be omitted. After some algebraic manipulations, we get (c).

Step 2: we average the conditional BER over Y. The BER of BPSK may then be written as follows:

$$\begin{aligned} \bar{P}_{BER} &= \sum_{m=1}^{N}\frac{B(m,1)}{4}\int_0^\infty \frac{1}{1+c\overline{\gamma}y}y^{m-1}e^{-y}dy \\ &= \sum_{m=1}^{N}\frac{B(m,1)}{4c\overline{\gamma}}\left[(-1)^{m-2}\left(\frac{1}{c\overline{\gamma}}\right)^{m-1}e^{\frac{1}{c\overline{\gamma}}}E_i\left(-\frac{1}{c\overline{\gamma}}\right)\right. \\ &\quad \left. + \sum_{k=1}^{m-1}\Gamma(k)\left(-\frac{1}{c\overline{\gamma}}\right)^{m-k-1}\right], \end{aligned} \tag{71}$$

where the integral is obtained by [37, eq. (3.353.5)].

APPENDIX E
PROOF OF PROPOSITION 7

To this end, we can further simplify the asymptotic result in (71). When the CSI is imperfect, $0 \leq \rho < 1$, the dominant part occurs when the number of antennas equals to one. Thus, only keeping the dominant part, we find

$$\begin{aligned} \bar{P}_{BER} &\approx \frac{\left(1-\rho^2\right)^{2(N-1)}}{4}\int_0^\infty \frac{e^{-y}}{1+c\overline{\gamma}y}dy \\ &\approx \frac{\left(1-\rho^2\right)^{2(N-1)}}{4}(c\overline{\gamma})^{-1}\left[\ln c\overline{\gamma} - \gamma_{EM}\right]. \end{aligned} \tag{72}$$

The derivation follows from Corollary 3.

When the CSI is estimated perfectly, $\rho = 1$, the value of $B(m, n)$ is not zero only when $m = N$ and $n = N$, so (70) can be further simplified as

$$\bar{P}_{BER|Y} \approx \frac{A(N)}{2N\sqrt{\pi}}\frac{\Gamma\left(N+\frac{1}{2}\right)}{(1+c\overline{\gamma}y)^N}. \tag{73}$$

By averaging this over the PDF of Y, we get

$$\begin{aligned} \bar{P}_{BER} &= \frac{\Gamma\left(N+\frac{1}{2}\right)}{2N\sqrt{\pi}\Gamma^2(N)}\int_0^\infty \frac{y^{N-1}e^{-y}}{(1+c\overline{\gamma}y)^N}dy \\ &\overset{(a)}{=} \frac{\Gamma\left(N+\frac{1}{2}\right)}{2N\sqrt{\pi}\Gamma(N)(tc\overline{\gamma})^N}\Psi\left(N, 1; \frac{1}{c\overline{\gamma}}\right), \end{aligned} \tag{74}$$

where (a) is obtained by applying [37, eq. (9.211.4)].

REFERENCES

[1] Y. Alsaba, S. K. A. Rahim, and C. Y. Leow, "Beamforming in wireless energy harvesting communications systems: A survey," *IEEE Commun. Surveys Tuts.*, vol. 20, no. 2, pp. 1329–1360, 2nd Quart., 2018.

[2] S. Ulukus *et al.*, "Energy harvesting wireless communications: A review of recent advances," *IEEE J. Sel. Areas Commun.*, vol. 33, no. 3, pp. 360–381, Mar. 2015.

[3] X. Lu, P. Wang, D. Niyato, D. I. Kim, and Z. Han, "Wireless networks with RF energy harvesting: A contemporary survey," *IEEE Commun. Surveys Tuts.*, vol. 17, no. 2, pp. 757–789, 2nd Quart., 2015.

[4] S. Bi, Y. Zeng, and R. Zhang, "Wireless powered communication networks: An overview," *IEEE Wireless Commun.*, vol. 23, no. 2, pp. 10–18, Apr. 2016.

[5] M. A. Hossain, R. M. Noor, K.-L. A. Yau, I. Ahmedy, and S. S. Anjum, "A survey on simultaneous wireless information and power transfer with cooperative relay and future challenges," *IEEE Access*, vol. 7, pp. 19166–19198, 2019.

[6] D. Niyato, D. I. Kim, M. Maso, and Z. Han, "Wireless powered communication networks: Research directions and technological approaches," *IEEE Trans. Wireless Commun.*, vol. 24, no. 6, pp. 88–97, Dec. 2017.

[7] *Powercast Product*, Powercast, Pittsburgh, PA, USA, 2020. [Online]. Available: https://www.powercastco.com/documentation/tx91501b-user-manual/

[8] Z. Mobini, M. Mohammadi, and C. Tellambura, "Wireless-powered full-duplex relay and friendly jamming for secure cooperative communications," *IEEE Trans. Inf. Forensics Security*, vol. 14, no. 3, pp. 621–634, Mar. 2019.

[9] W. Huang, H. Chen, Y. Li, and B. Vucetic, "On the performance of multi-antenna wireless-powered communications with energy beamforming," *IEEE Trans. Veh. Technol.*, vol. 65, no. 3, pp. 1801–1808, Mar. 2016.

[10] Z. Chu, F. Zhou, Z. Zhu, M. Sun, and N. Al-Dhahir, "Energy beamforming design and user cooperation for wireless powered communication networks," *IEEE Wireless Commun. Lett.*, vol. 6, no. 6, pp. 750–753, Dec. 2017.

[11] H. Ju and R. Zhang, "Throughput maximization in wireless powered communication networks," *IEEE Trans. Wireless Commun.*, vol. 13, no. 1, pp. 418–428, Jan. 2014.

[12] N. Deepan and B. Rebekka, "On the performance of wireless powered communication networks over generalized κ —μ fading channels," *Phys. Commun.*, vol. 36, Oct. 2019, Art. no. 100759.

[13] Y. Gao, Y. Chen, Y. Zhou, and N. Cao, "BER and achievable rate analysis of wireless powered communications with correlated uplink and downlink," *IET Commun.*, vol. 12, no. 3, pp. 310–316, Feb. 2018.

[14] A. Almradi, "Information and energy beamforming in MIMO wireless powered systems," in *Proc. IEEE Global Commun. Conf. (GLOBECOM)*, Washington, DC, USA, 2016, pp. 1–7.

[15] X. Chen, X. Wang, and X. Chen, "Energy-efficient optimization for wireless information and power transfer in large-scale MIMO systems employing energy beamforming," *IEEE Commun. Lett.*, vol. 2, no. 6, pp. 667–670, Dec. 2013.

[16] G. Wang, Q. Liu, R. He, F. Gao, and C. Tellambura, "Acquisition of channel state information in heterogeneous cloud radio access networks: Challenges and research directions," *IEEE Wireless Commun.*, vol. 22, no. 3, pp. 100–107, Jun. 2015.

[17] G. Wang, F. Gao, Y.-C. Wu, and C. Tellambura, "Joint CFO and channel estimation for OFDM-based two-way relay networks," *IEEE Trans. Wireless Commun.*, vol. 10, no. 2, pp. 456–465, Feb. 2011.

[18] G. Pan *et al.*, "On secrecy performance of MISO SWIPT systems with TAS and imperfect CSI," *IEEE Trans. Commun.*, vol. 64, no. 3, pp. 3831–3843, Sep. 2016.

[19] S. Schiessl, H. Al-Zubaidy, M. Skoglund, and J. Gross, "Delay performance of wireless communications with imperfect CSI and finite-length coding," *IEEE Trans. Commun.*, vol. 66, no. 12, pp. 6527–6541, Dec. 2018.

[20] K. S. Ahn, S.-W. Choi, and J.-M. Ahn, "Secrecy performance of maximum ratio diversity with channel estimation error," *IEEE Signal Process. Lett.*, vol. 22, no. 11, pp. 2167–2171, Nov. 2015.

[21] M. J. Gans, "The effect of Gaussian error in maximal ratio combiners," *IEEE Trans. Commun. Technol.*, vol. 19, no. 4, pp. 492–500, Aug. 1971.

[22] B. R. Tomiuk, N. C. Beaulieu, and A. A. Abu-Dayya, "General forms for maximal ratio diversity with weighting errors," *IEEE Trans. Commun.*, vol. 47, no. 4, pp. 488–492, Apr. 1999.

[23] Z. Chang, Z. Wang, X. Guo, Z. Han, and T. Ristaniemi, "Energy-efficient resource allocation for wireless powered massive MIMO system with imperfect CSI," *IEEE Trans. Green Commun. Netw.*, vol. 1, no. 2, pp. 121–130, Jun. 2017.

[24] Y. Huang, P. Zhang, Q. Wu, and J. Wang, "Secrecy performance of wireless powered communication networks with multiple eavesdroppers and outdated CSI," *IEEE Access*, vol. 6, pp. 33774–33788, 2018.

[25] Y. Wu, X. Chen, C. Yuen, and C. Zhong, "Robust resource allocation for secrecy wireless powered communication networks," *IEEE Commun. Lett.*, vol. 20, no. 12, pp. 2430–2433, Dec. 2016.

[26] F. Zhao, H. Lin, C. Zhong, Z. Hadzi-Velkov, G. K. Karagiannidis, and Z. Zhang, "On the capacity of wireless powered communication systems over Rician fading channels," *IEEE Trans. Commun.*, vol. 66, no. 1, pp. 404–417, Jan. 2018.

[27] G. Yang, C. K. Ho, R. Zhang, and Y. L. Guan, "Throughput optimization for massive MIMO systems powered by wireless energy transfer," *IEEE J. Sel. Areas Commun.*, vol. 33, no. 8, pp. 1640–1650, Aug. 2015.

[28] H. Liang, C. Zhong, X. Chen, H. A. Suraweera, and Z. Zhang, "Wireless powered dual-hop multi-antenna relaying systems: Impact of CSI and antenna correlation," *IEEE Trans. Wireless Commun.*, vol. 16, no. 4, pp. 2505–2519, Apr. 2017.

[29] J. Zhang and G. Pan, "Outage analysis of wireless-powered relaying MIMO systems with non-linear energy harvesters and imperfect CSI," *IEEE Access*, vol. 4, pp. 7046–7053, 2016.

[30] J. Ye *et al.*, "Cooperative communications with wireless energy harvesting over Nakagami-*m* fading channels," *IEEE Trans. Commun.*, vol. 65, no. 12, pp. 5149–5164, Dec. 2017.

[31] Y. Liu, K.-W. Chin, and C. Yang, "Uplinks schedulers for RF-energy harvesting networks with imperfect CSI," *IEEE Trans. Veh. Technol.*, vol. 69, no. 4, pp. 4233–4245, Apr. 2020.

[32] X. Liu, Y. Gao, M. Guo, and N. Sha, "Secrecy throughput optimization for the WPCNs with non-linear EH model," *IEEE Access*, vol. 7, pp. 59477–59490, 2019.

[33] Z. Wang and G. Giannakis, "A simple and general parameterization quantifying performance in fading channels," *IEEE Trans. Commun.*, vol. 51, no. 8, pp. 1389–1398, Aug. 2003.

[34] Y. Dhungana and C. Tellambura, "New simple approximations for error probability and outage in fading," *IEEE Commun. Lett.*, vol. 16, no. 11, pp. 1760–1763, Nov. 2012.

[35] Y. Dhungana and C. Tellambura, "Uniform approximations for wireless performance in fading channels," *IEEE Commun. Lett.*, vol. 61, no. 11, pp. 4768–4779, Nov. 2013.

[36] V. R. S. Banjade, C. Tellambura, and H. Jiang, "Asymptotic performance of energy detector in fading and diversity reception," *IEEE Trans. Commun.*, vol. 63, no. 6, pp. 2031–2043, Jun. 2015.

[37] I. S. Gradshteyn and I. M. Ryzhik, *Table of Integrals, Series, and Products, 7th edition*. Boston, MA, USA: Academic, 2007.

[38] M. Taghadosi, L. Albasha, N. A. Quadir, Y. A. Rahama, and N. Qaddoumi, "High efficiency energy harvesters in 65nm CMOS process for autonomous IoT sensor applications," *IEEE Access*, vol. 6, pp. 2397–2409, 2017.

[39] C. Tellamura, A. Annamalai, and V. Bhargava, "Closed form and infinite series solutions for the MGF of a dual-diversity selection combiner output in bivariate Nakagami fading," *IEEE Trans. Commun.*, vol. 51, no. 4, pp. 539–542, Apr. 2003.

[40] B. M. Hochwald, T. L. Marzetta, and V. Tarokh, "Multiple-antenna channel hardening and its implications for rate feedback and scheduling," *IEEE Trans. Inf. Theory*, vol. 50, no. 9, pp. 1893–1909, Sep. 2004.

[41] T. L. Marzetta, E. G. Larsson, H. Yang, and H. Q. Ngo, *Fundamentals of Massive MIMO*, 1st ed. Cambridge, U.K.: Cambridge Univ. Press, 2016.

[42] K. Huang and V. K. N. Lau, "Enabling wireless power transfer in cellular networks: Architecture, modeling and deployment," *IEEE Trans. Wireless Commun.*, vol. 13, no. 2, pp. 902–912, Feb. 2014.

[43] I. Chatzigeorgiou, "Bounds on the Lambert function and their application to the outage analysis of user cooperation," *IEEE Commun. Lett.*, vol. 17, no. 8, pp. 1505–1508, Aug. 2013.
[44] S.-N. Jin, D.-W. Yue, and H. H. Nguyen, "Power scaling laws of massive MIMO full-duplex relaying with hardware impairments," *IEEE Access*, vol. 6, pp. 40860–40882, 2018.
[45] S. Silva, G. A. A. Baduge, M. Ardakani, and C. Tellambura, "Performance analysis of massive MIMO two-way relay networks with pilot contamination, imperfect CSI, and antenna correlation," *IEEE Trans. Veh. Technol.*, vol. 67, no. 6, pp. 4831–4842, Jun. 2018.
[46] P. S. Bithas, N. C. Sagias, P. T. Mathiopoulos, G. K. Karagiannidis, and A. A. Rontogiannis, "On the performance analysis of digital communications over generalized-K fading channels," *IEEE Commun. Lett.*, vol. 10, no. 5, pp. 353–355, May 2006.
[47] C. Tellambura, "Evaluation of the exact union bound for trellis-coded modulations over fading channels," *IEEE Trans. Commun.*, vol. 44, no. 12, pp. 1693–1699, Dec. 1996.
[48] C. Tellambura and A. J. Mueller, and V. K. Bhargava, "Analysis of M-ary phase-shift keying with diversity reception for land-mobile satellite channels," *IEEE Trans. Veh. Technol.*, vol. 46, no. 4, pp. 910–922, Nov. 1997.
[49] H. Shin and J. H. Lee, "Performance analysis of space-time block codes over keyhole Nakagami-*m* fading channels," *IEEE Trans. Veh. Technol.*, vol. 53, no. 2, pp. 351–362, Mar. 2004.
[50] Y. Chen and C. Tellambura, "Distribution functions of selection combiner output in equally correlated Rayleigh, Rician, and Nakagami-*m* fading channels," *IEEE Trans. Commun.*, vol. 52, no. 11, pp. 1948–1956, Nov. 2004.
[51] H. Lei, Y. Zhang, K.-H. Park, I. S. Ansari, G. Pan, and M.-S. Alouini, "Performance analysis of dual-hop RF-UWOC systems," *IEEE Photon. J.*, vol. 12, no. 2, pp. 1–15, Apr. 2020.
[52] E. Boshkovska, D. W. K. Ng, N. Zlatanov, and R. Schober, "Practical non-linear energy harvesting model and resource allocation for SWIPT systems," *IEEE Commun. Lett.*, vol. 19, no. 12, pp. 2082–2085, Dec. 2015.

DANYANG WANG (Graduate Student Member, IEEE) received the B.S. degree from Southwest University, China, in 2017. She is currently pursuing the M.Sc. degree with the University of Alberta, Edmonton, AB, Canada. Her research interests are in the areas of wireless communications, including wireless energy harvesting and physical layer security.

CHINTHA TELLAMBURA (Fellow, IEEE) received the B.Sc. degree (First Class Hons.) from the University of Moratuwa, Sri Lanka, the M.Sc. degree in electronics from King's College, University of London, U.K., and the Ph.D. degree in electrical engineering from the University of Victoria, Canada.

He was with Monash University, Australia, from 1997 to 2002. He is currently a Professor with the Department of Electrical and Computer Engineering, University of Alberta. He has authored or coauthored over 500 journal and conference papers with an H-index of 76 (Google Scholar). His current research interests include the design, modelling, and analysis of current and future wireless networks.

Prof. Tellambura has received best paper awards in the Communication Theory Symposium in 2012 IEEE International Conference on Communications (ICC), Canada, and 2017 ICC, France. He is the winner of the prestigious McCalla Professorship and the Killam Annual Professorship from the University of Alberta. He served as an Editor for the IEEE TRANSACTIONS ON COMMUNICATIONS from 1999 to 2011, and the IEEE TRANSACTIONS ON WIRELESS COMMUNICATIONS from 2001 to 2007, and for the latter he was the Area Editor for Wireless Communications Systems and Theory from 2007 to 2012. In 2011, he was elected as an IEEE Fellow for his contributions to physical layer wireless communication theory. In 2017, he was elected as a Fellow of Canadian Academy of Engineering.